LA-UR-05-2686

*Approved for public release; distribution is unlimited.*

*Title:* CEM03.01 and LAQGSM03.01 Versions of the Improved Cascade-Exciton Model (CEM) and Los Alamos Quark-Gluon String Model (LAQGSM) Codes

*Author(s):* S. G. Mashnik, K. K. Gudima, M. I. Baznat, A. J. Sierk, R. E. Prael, and N. V. Mokhov

*Submitted to:* Distribution

**Los Alamos**
NATIONAL LABORATORY
**research note**

Applied Physics Division, X
Diagnostic Applications Group, X-5

*To/MS:* Distribution
*From/MS:* S. G. Mashnik, X-5, MS B283
*Phone/FAX:* 7-9946/7-1931
*Email:* mashnik@lanl.gov
*Symbol:* X-5-RN(U)05-11/LA-UR-05-2686
*Date:* March 31, 2005

# CEM03.01 and LAQGSM03.01 versions of the improved Cascade-Exciton Model (CEM) and Los Alamos Quark-Gluon String Model (LAQGSM) Codes

**Abstract**

This Research Note presents a summary and progress report on development of the CEM03.01 and LAQGSM03.01 versions of the improved Cascade-Exciton Model (CEM) and Los Alamos Quark-Gluon String Model (LAQGSM) codes as event generators for the MCNP6, MARS, and MCNPX transport codes. Part of the work described here was performed by Dr. K. K. Gudima of the Institute of Applied Physics, Academy of Science of Moldova, during his visit and work with Stepan Mashnik (X-5) at LANL from October 4 to December 22, 2004. The other part was performed before and after this period by Stepan Mashnik in collaboration with Arnie Sierk (T-16) and Dick Prael (X-5), Kostea Gudima and Mircea Baznat of IAP, AS, Moldova, and with Nikolai Mokhov of FNAL. This work was funded by the Los Alamos National Laboratory and partially, by NASA, CRDF, and the RIA project.

## 1. Introduction

The process of determining the feasibility of Proton Radiography (PRAD) as the radiographic probe for the Advanced Hydro-test Facility as well as its design and operation require information about spectra of secondary particles and isotopes produced by high energy protons interacting in the target and structural materials. Reliable models and codes are needed to provide such data. One of the best candidates for high-energy codes that may be used in simulations for PRAD is the Los Alamos version of the Quark-Gluon String Model, LAQGSM, developed recently by K. K. Gudima in collaboration with S. G. Mashnik and A. J. Sierk. On the other hand, to describe reactions at lower energies (below about 5 GeV) that are induced by secondary particles produced by the bombarding beam of 50 GeV protons on PRAD targets, the improved Cascade-Exciton Model code CEM2k developed recently at LANL by the same authors proves to have one of the best predictive powers in comparison with other available codes. This is why a serious interest in our models and codes and a wish to partially fund their further development and improvement were shown by several outside organizations, like the

National Aeronautics and Space Agency (NASA), the U. S. Civilian Research and Development Foundation (CRDF), and the Rare Isotope Accelerator (RIA) project.

The 2003 versions of CEM2k and LAQGSM [1, 2] describe nuclear reactions much better than their precursors. They have been benchmarked on a variety of particle-particle, particle-nucleus, and nucleus-nucleus reactions at energies from 10 MeV to 800 GeV per nucleon, and have have been incorporated as event generators into the transport codes MARS, MCNPX, and a working version of LAHET. This does not means that our codes are perfect and do not have any problems. For instance,

A) Both CEM2k and LAQGSM had some problems in a correct description of the experimental spectra of forward-emitted nucleons, just as all other models based on an IntraNuclear Cascade (INC) do (see [3] for more details);

B) CEM2k and LAQGSM had some problems in a correct description of complex particle (d, t, $^3$He, and $^4$He) double-differential cross sections, just as other currently available models do;

C) CEM2k was able to describe reactions induced by photons at energies only up to about 1.5 GeV, while LAQGSM did not consider photonuclear reactions at all.

Further improvements, verification, and validation of the CEM2k and LAQGSM codes were necessary to assure that we have reliable tools for simulations needed for PRAD and other LANL/DOE applications. This was the main reason why we invited Dr. Gudima to work with us in 2004 at LANL on further development of the codes CEM2k and LAQGSM; solving the three problems listed above was the main aim of the work presented here.

## 2. Results

The work proceeded well, all planned problems were solved, and the project was completed with the following main results and deliverables:

1) The problem of a correct description of the experimental spectra of forward-emitted nucleons was addressed and partially solved in CEM03 and LAQGSM03 [3] by developing new approximations to describe more accurately experimental elementary energy and angular distributions of secondary particles from hadron-hadron and photon-hadron interactions using available data and approximations published by other authors; details and results on this work may be found in [3, 4].

2) Improvement of the description of the d, t, $^3$He, and $^4$He spectra and yields were solicited from us (and partially funded) by Dick Olsher and Thomas McLean of HSR-4: They need reliable tools to predict complex-particle spectra from a number of reactions for their work on developing a portable high-energy neutron spectrometer. Such an improvement is important also for other applications like estimating gas production in targets and structural materials at different facilities etc., therefore we have addressed this problem with care: First, we have fitted the probability of several excited nucleons ("excitons") coalescing into a complex particle at the

preequilibrium stage of a nuclear reaction, trying to describe as well as possible all available experimental complex-particle spectra. Then we developed a method of extrapolating/interpolating the fitted values to arbitrary reactions, in a similar manner to the way we had previously described fission cross sections [5]. This allows us to describe quite well and much better than with previous versions of our codes angle-integrated energy spectra of complex particles from a variety of reactions. To properly describe double-differential cross sections of complex particles, we have incorporated into both CEM03 and LAQGSM03 the known systematics by Kalbach. Figs. 1 and 2 show examples of angle-integrated energy spectra (Fig. 1) and double-differential cross sections of recently measured 62.9 MeV p + $^{208}$Pb reactions [6] compared with our CEM03.01 results. We see that CEM03.01 describes these particle spectra very well. Comparing our results with calculations by the CERN transport code FLUKA of Alfredo Ferrari *et al.*, as published in [6], the Liege INC by Joseph Cugnon *et al.* merged with the GSI evaporation/fission model ABLA by Karl-Hans Schmidt *et al.* in the code INCL4+ABLA, with the recent microscopic model TALYS by Arjan Koning *et al.*, and with the older LANL microscopic model GNASH by Mark Chadwick *et al.*, one can see that CEM03.01 describes these data not only better than FLUKA and INCL4, but also not worse and for some reactions even better than the microscopic models TALYS and GNASH, developed especially to describe reactions at such relatively low energies and to produce data libraries up to 150 MeV for transport codes.

We note that all the CEM03.01 and LAQGSM03.01 results shown in Figs. 1 and 2 and in all following figures are obtained using final, fixed default values of all parameters, without fitting these data. We only specify in the inputs to CEM03.01 and LAQGSM03.01 the energy of the incident projectiles and $A$ and $Z$ of the target, then calculate, just as is done when our event generators are used in transport codes.

Fig. 3 shows one more example of complex particle spectra at higher energies, above the threshold for pion production where microscopic models like TALYS and GNASH can not be applied, namely the spectra of $^{4}$He and $^{3}$He emitted from interaction of 210-, 300-, and 480-MeV protons with Ag [7]. One can see that CEM03.01 also describes these reactions quite well. The same reactions were analyzed with LAQGSM03.01, whose results for complex particle spectra are very similar to those of CEM03.01.

This part of our present work will be presented in detail in a future publication.

3) Our FNAL collaborator and author of the MARS transport code, Nikolai Mokhov, called our attention to some problems in a correct description by CEM03 of pion spectra (especially, of $\pi^+$) from some proton-induced reactions near 1 GeV. Investigating this problem, we found that it was related to the use of a rough approximation for the momenta of secondary pions produced in elementary interactions with three particles in the final state. We addressed this problem in CEM03.01 and improved the description of pion spectra from such reactions; Fig. 4 demonstrates this for $\pi^+$ spectra emitted from interactions of 730 MeV protons with C, Al, Cu, and Pb nuclei [8]. Similar results were obtained for other reactions.

4) After making the improvements to the INC and preequilibrium parts of CEM (and LAQGSM) as described above in 1–3), the mean values of the mass and charge numbers, $A$ and $Z$ of the excited compound nuclei produced after the preequilibrium stage of nuclear reactions and their mean excitation energy, $E^*$, have changed slightly, which affects the probability of heavy compound nuclei (especially of preactinides) to fission. This means that the procedure of fitting the ratio of the level-density parameters of fissioning nuclei at the saddle point, $a_f$, and for evaporation from compound nuclei, $a_n$, *i.e.*, $a_f/a_n$ which we performed in [5] to provide the best description by CEM2k and LAQGSM of fission cross sections is no longer correct. We redid for CEM03.01 and LAQGSM03.01 the determination of the level-density ratio done in [5] for CEM2k and LAQGSM, ensuring that the latest versions of our codes describe as well as possible fission cross sections from various reactions. Figs. 5 and 6 show examples of fission cross sections for proton- and neutron-induced reactions on $^{209}$Bi, $^{208,207,206,204}$Pb, and $^{205}$Tl. One can see that CEM03.01 reproduces perfectly the recent Uppsala measurements [9, 10] of proton-induced fission cross sections and also agrees reasonably well with the recent Uppsala [9, 11, 13] and Saint-Petersburg [12] data and older measurements at LANL by Parrish Staples *et al.* [14] for neutron-induced fission cross sections. Results by LAQGSM03.01 for these and other fission cross sections practically coincide with ones by CEM03.01, as is expected from the fitting process [5]. Some of our current results on fission cross sections for photonuclear reactions were published in [4]; results for nucleon-induced reactions will be published in a future paper.

5) Both CEM03 and LAQGSM codes were extended to describe a previously unconsidered type of photonuclear reaction, namely those induced by bremsstrahlung photons. In contrast to reactions induced by monoenergetic photons of a given energy $E$, the bremsstrahlung beam is produced by monoenergetic electrons and has a spectrum of photon energies $E$ of the form $N(E, E_0) \sim 1/E$, from 0 to $E_0$, where the end-point energy $E_0$ is the maximum energy of photons produced by the given electron beam. This work is described in detail in our recent paper [4]. Figs. 7 and 8 demonstrate that CEM03.01 allows us to describe reasonably well many photonuclear reactions needed for applications, as well as to analyze mechanisms of photonuclear reactions for fundamental studies (see [4] for more details).

6) To understand better the dynamics of fission and mechanisms of nuclear reactions in general, following a suggestion by Andre Michaudon of LANSCE-3, we have considerably extended the information printed in the outputs of both CEM03.01 and LAQGSM03.01 as compared with their precursors. So in addition to tables of particle spectra, their multiplicities and mean energies, and cross sections for all products, we included in the outputs of the recent versions tables for the product yields separately for forward- and backward-emitted nuclei. We also included similar tables for the mean kinetic energy of all products, tables with $A$- and $Z$-distributions of their mean emission angle, z-velocity, and for the ratio forward/backward. Additionally, we added tables with the mass and charge distributions of nuclei after the cascade and preequilibrium stages of reactions: for all nuclei, for ones that do not fission, for ones that fission, and for the last group, just before fission, *i.e.*, when several "pre-fission" particles were emitted at the cascade, preequilibrium, and evaporation stages of nuclear reactions before

fission. We added tables with distributions of nuclei according to their excitation energy, linear momentum, and angular momentum and with distributions of fission-fragment opening angles in the laboratory system in different bins of neutron multiplicity, *i.e.*, for all events and for events with the neutron multiplicity, $< n >$, $< n >= 0 - 5$, $< n >= 6 - 8$, $< n >= 9 - 12$, $< n >= 13 - 15$, $< n >= 16 - 19$, and for $< n > > 19$. Finally, we added tables with distributions of neutron multiplicities: for all stages of of a reaction (total), for Cascade, Preequilibrium, and evaporation events that do not fission ("evap. res."), for evaporation neutrons before fission ("pre-fiss."), and for evaporation of neutrons from fission fragments ("post-fiss."). We believe that this part of our work is very useful for better understanding the mechanisms of nuclear reactions and for developing better event generators in the future.

Figs. 9 and 10 show two examples of such results; examples of results for other characteristics of nuclear reactions from this part of our work may be found in our recent paper [4].

7) The initial version of LAQGSM did not consider photonuclear reactions at all, while its 2003 version, LAQGSM03 and CEM03.01 describe such reactions only for energies up to about 1.5 GeV. This is not convenient when using our codes to solve problems for PRAD, NASA, and other high-energy applications or to analyze future high-energy measurements at the Thomas Jefferson National Accelerator Facility (CEBAF), where photons with much higher energy are created and need to be simulated by an event generator in a transport code. To address this problem, we have extended LAQGSM03 to describe photonuclear reactions at energies up to tens of GeV. For this, we took advantage of the high-energy event generators for $\gamma p$ and $\gamma n$ elementary interactions from the Moscow high-energy photonuclear reaction model [16] kindly sent us by one of its co-authors, Dr. Igor Pshenichnov. We have incorporated into LAQGSM03.01 56 channels to consider $\gamma p$ elementary interactions during the cascade stage of reactions, and 56 channels for $\gamma n$ interactions. These reaction channels new to LAQGSM03.01 are listed in Table 1 (its precursor, LAQGSM03 [4], considers only channels #1–3 and 15–17, and only up to about 1.5 GeV). To describe in LAQGSM03.01 the two-body channels #1–14, we use part of a file containing smooth approximations through presently available experimental data sent us by Dr. Pshenichnov and have written an algorithm to simulate unambiguously $d\sigma/d\Omega$ and to choose the corresponding value of $\Theta$ for any $E_\gamma$, using a single random number $\xi$ uniformly distributed in the interval [0,1], as described in [4]. To describe the channels #15–21 with two and three pions in the final state, we use the $\gamma p$ and $\gamma n$ event generators send us by Dr. Pshenichnov, but use our own interpolation for integral cross sections. Finally, we describe in LAQGSM03.01 the multi-pion channels #22–56 using the isospin statistical model as realized in the $\gamma p$ and $\gamma n$ event generators send us by Dr. Pshenichnov and described in [16], without any changes. LAQGSM03.01, extended in this manner, allows us to describe well photonuclear reactions at energies both below $\sim 1.5$ GeV where its precursor LAQGSM03 and CEM03.01 do work (see Fig. 11 for one example), and at higher photon energies (see Figs. 12–16). We note that to the best of our knowledge, we are able to describe with LAQGSM03.01 the data shown in Figs. 12–16 for the first time; we do not know of any publication or oral presentation where these measurements were reproduced by a theoretical model, event generator, or transport code.

This part of our work will be presented in detail in a future publication.

Table 1. Channels of elementary $\gamma N$ interactions taken into account in LAQGSM03.01

| # | $\gamma p$-interactions | $\gamma n$-interactions |
|---|---|---|
| 1 | $\gamma p \to \pi^+ n$ | $\gamma n \to \pi^- p$ |
| 2 | $\gamma p \to \pi^0 n$ | $\gamma n \to \pi^0 n$ |
| 3 | $\gamma p \to \Delta^{++} \pi^-$ | $\gamma n \to \Delta^+ \pi^-$ |
| 4 | $\gamma p \to \Delta^+ \pi^0$ | $\gamma n \to \Delta^0 \pi^0$ |
| 5 | $\gamma p \to \Delta^0 \pi^+$ | $\gamma n \to \Delta^- \pi^+$ |
| 6 | $\gamma p \to \rho^0 p$ | $\gamma n \to \rho^0 n$ |
| 7 | $\gamma p \to \rho^+ n$ | $\gamma n \to \rho^- p$ |
| 8 | $\gamma p \to \eta p$ | $\gamma n \to \eta n$ |
| 9 | $\gamma p \to \omega p$ | $\gamma n \to \omega n$ |
| 10 | $\gamma p \to \Lambda K^+$ | $\gamma n \to \Lambda K^0$ |
| 11 | $\gamma p \to \Sigma^0 K^+$ | $\gamma n \to \Sigma^0 K^0$ |
| 12 | $\gamma p \to \Sigma^+ K^0$ | $\gamma n \to \Sigma^- K^+$ |
| 13 | $\gamma p \to \eta' p$ | $\gamma n \to \eta' n$ |
| 14 | $\gamma p \to \phi p$ | $\gamma n \to \phi n$ |
| 15 | $\gamma p \to \pi^+ \pi^- p$ | $\gamma n \to \pi^+ \pi^- n$ |
| 16 | $\gamma p \to \pi^0 \pi^+ n$ | $\gamma n \to \pi^0 \pi^- p$ |
| 17 | $\gamma p \to \pi^0 \pi^0 p$ | $\gamma n \to \pi^0 \pi^0 n$ |
| 18 | $\gamma p \to \pi^0 \pi^0 \pi^0 p$ | $\gamma n \to \pi^0 \pi^0 \pi^0 n$ |
| 19 | $\gamma p \to \pi^+ \pi^- \pi^0 p$ | $\gamma n \to \pi^+ \pi^- \pi^0 n$ |
| 20 | $\gamma p \to \pi^+ \pi^0 \pi^0 n$ | $\gamma n \to \pi^- \pi^0 \pi^0 p$ |
| 21 | $\gamma p \to \pi^+ \pi^+ \pi^- n$ | $\gamma n \to \pi^+ \pi^- \pi^- p$ |
| 22 | $\gamma p \to \pi^0 \pi^0 \pi^0 \pi^0 p$ | $\gamma n \to \pi^0 \pi^0 \pi^0 \pi^0 n$ |
| 23 | $\gamma p \to \pi^+ \pi^- \pi^0 \pi^0 p$ | $\gamma n \to \pi^+ \pi^- \pi^0 \pi^0 n$ |
| 24 | $\gamma p \to \pi^+ \pi^+ \pi^- \pi^- p$ | $\gamma n \to \pi^+ \pi^+ \pi^- \pi^- n$ |
| 25 | $\gamma p \to \pi^+ \pi^0 \pi^0 \pi^0 n$ | $\gamma n \to \pi^- \pi^0 \pi^0 \pi^0 p$ |
| 26 | $\gamma p \to \pi^+ \pi^+ \pi^- \pi^0 n$ | $\gamma n \to \pi^+ \pi^- \pi^- \pi^0 p$ |
| 27 | $\gamma p \to \pi^0 \pi^0 \pi^0 \pi^0 \pi^0 p$ | $\gamma n \to \pi^0 \pi^0 \pi^0 \pi^0 \pi^0 n$ |
| 28 | $\gamma p \to \pi^+ \pi^- \pi^0 \pi^0 \pi^0 p$ | $\gamma n \to \pi^+ \pi^- \pi^0 \pi^0 \pi^0 n$ |
| 29 | $\gamma p \to \pi^+ \pi^+ \pi^- \pi^- \pi^0 p$ | $\gamma n \to \pi^+ \pi^+ \pi^- \pi^- \pi^0 n$ |
| 30 | $\gamma p \to \pi^+ \pi^0 \pi^0 \pi^0 \pi^0 n$ | $\gamma n \to \pi^- \pi^0 \pi^0 \pi^0 \pi^0 p$ |
| 31 | $\gamma p \to \pi^+ \pi^+ \pi^- \pi^0 \pi^0 n$ | $\gamma n \to \pi^+ \pi^- \pi^- \pi^0 \pi^0 p$ |
| 32 | $\gamma p \to \pi^+ \pi^+ \pi^+ \pi^- \pi^- n$ | $\gamma n \to \pi^+ \pi^+ \pi^- \pi^- \pi^- p$ |

Table 1 (continuation). Channels of elementary $\gamma N$ interactions taken into account in LAQGSM03.01

| # | $\gamma p$-interactions | $\gamma n$-interactions |
|---|---|---|
| 33 | $\gamma p \to \pi^0\pi^0\pi^0\pi^0\pi^0\pi^0 p$ | $\gamma n \to \pi^0\pi^0\pi^0\pi^0\pi^0\pi^0 n$ |
| 34 | $\gamma p \to \pi^+\pi^-\pi^0\pi^0\pi^0\pi^0 p$ | $\gamma n \to \pi^+\pi^-\pi^0\pi^0\pi^0\pi^0 n$ |
| 35 | $\gamma p \to \pi^+\pi^+\pi^-\pi^-\pi^0\pi^0 p$ | $\gamma n \to \pi^+\pi^+\pi^-\pi^-\pi^0\pi^0 n$ |
| 36 | $\gamma p \to \pi^+\pi^+\pi^+\pi^-\pi^-\pi^- p$ | $\gamma n \to \pi^+\pi^+\pi^+\pi^-\pi^-\pi^- n$ |
| 37 | $\gamma p \to \pi^+\pi^0\pi^0\pi^0\pi^0\pi^0 n$ | $\gamma n \to \pi^-\pi^0\pi^0\pi^0\pi^0\pi^0 p$ |
| 38 | $\gamma p \to \pi^+\pi^+\pi^-\pi^0\pi^0\pi^0 n$ | $\gamma n \to \pi^+\pi^-\pi^-\pi^0\pi^0\pi^0 p$ |
| 39 | $\gamma p \to \pi^+\pi^+\pi^+\pi^-\pi^-\pi^0 n$ | $\gamma n \to \pi^+\pi^+\pi^-\pi^-\pi^-\pi^0 p$ |
| 40 | $\gamma p \to \pi^0\pi^0\pi^0\pi^0\pi^0\pi^0\pi^0 p$ | $\gamma n \to \pi^0\pi^0\pi^0\pi^0\pi^0\pi^0\pi^0 n$ |
| 41 | $\gamma p \to \pi^+\pi^-\pi^0\pi^0\pi^0\pi^0\pi^0 p$ | $\gamma n \to \pi^+\pi^-\pi^0\pi^0\pi^0\pi^0\pi^0 n$ |
| 42 | $\gamma p \to \pi^+\pi^+\pi^-\pi^-\pi^0\pi^0\pi^0 p$ | $\gamma n \to \pi^+\pi^+\pi^-\pi^-\pi^0\pi^0\pi^0 n$ |
| 43 | $\gamma p \to \pi^+\pi^+\pi^+\pi^-\pi^-\pi^-\pi^0 p$ | $\gamma n \to \pi^+\pi^+\pi^+\pi^-\pi^-\pi^-\pi^0 n$ |
| 44 | $\gamma p \to \pi^+\pi^0\pi^0\pi^0\pi^0\pi^0\pi^0 n$ | $\gamma n \to \pi^-\pi^0\pi^0\pi^0\pi^0\pi^0\pi^0 p$ |
| 45 | $\gamma p \to \pi^+\pi^+\pi^-\pi^0\pi^0\pi^0\pi^0 n$ | $\gamma n \to \pi^+\pi^-\pi^-\pi^0\pi^0\pi^0\pi^0 p$ |
| 46 | $\gamma p \to \pi^+\pi^+\pi^+\pi^-\pi^-\pi^0\pi^0 n$ | $\gamma n \to \pi^+\pi^+\pi^-\pi^-\pi^-\pi^0\pi^0 p$ |
| 47 | $\gamma p \to \pi^+\pi^+\pi^+\pi^+\pi^-\pi^-\pi^- n$ | $\gamma n \to \pi^+\pi^+\pi^+\pi^-\pi^-\pi^-\pi^- p$ |
| 48 | $\gamma p \to \pi^0\pi^0\pi^0\pi^0\pi^0\pi^0\pi^0\pi^0 p$ | $\gamma n \to \pi^0\pi^0\pi^0\pi^0\pi^0\pi^0\pi^0\pi^0 n$ |
| 49 | $\gamma p \to \pi^+\pi^-\pi^0\pi^0\pi^0\pi^0\pi^0\pi^0 p$ | $\gamma n \to \pi^+\pi^-\pi^0\pi^0\pi^0\pi^0\pi^0\pi^0 n$ |
| 50 | $\gamma p \to \pi^+\pi^+\pi^-\pi^-\pi^0\pi^0\pi^0\pi^0 p$ | $\gamma n \to \pi^+\pi^+\pi^-\pi^-\pi^0\pi^0\pi^0\pi^0 n$ |
| 51 | $\gamma p \to \pi^+\pi^+\pi^+\pi^-\pi^-\pi^-\pi^0\pi^0 p$ | $\gamma n \to \pi^+\pi^+\pi^+\pi^-\pi^-\pi^-\pi^0\pi^0 n$ |
| 52 | $\gamma p \to \pi^+\pi^+\pi^+\pi^+\pi^-\pi^-\pi^-\pi^- p$ | $\gamma n \to \pi^+\pi^+\pi^+\pi^+\pi^-\pi^-\pi^-\pi^- n$ |
| 53 | $\gamma p \to \pi^+\pi^0\pi^0\pi^0\pi^0\pi^0\pi^0\pi^0 n$ | $\gamma n \to \pi^-\pi^0\pi^0\pi^0\pi^0\pi^0\pi^0\pi^0 p$ |
| 54 | $\gamma p \to \pi^+\pi^+\pi^-\pi^0\pi^0\pi^0\pi^0\pi^0 n$ | $\gamma n \to \pi^+\pi^-\pi^-\pi^0\pi^0\pi^0\pi^0\pi^0 p$ |
| 55 | $\gamma p \to \pi^+\pi^+\pi^+\pi^-\pi^-\pi^0\pi^0\pi^0 n$ | $\gamma n \to \pi^+\pi^+\pi^-\pi^-\pi^-\pi^0\pi^0\pi^0 p$ |
| 56 | $\gamma p \to \pi^+\pi^+\pi^+\pi^+\pi^-\pi^-\pi^-\pi^0 n$ | $\gamma n \to \pi^+\pi^+\pi^+\pi^-\pi^-\pi^-\pi^-\pi^0 p$ |

8) Finally, we have benchmarked the new versions of our codes on a variety of particle-particle, particle-nucleus, and nucleus-nucleus reactions at energies from 10 MeV to 800 GeV per nucleon and found that they describe reactions generally much better than their precursors. Two examples of this part of our work are shown in Figs. 17 and 18. We note that the 400 GeV experimental data [25]–[27] compared in Fig. 17 with our LAQGSM03.01 results are described here for the first time: Though these data were measured at FNAL 25 years ago, we do not know any publication or oral presentation where these measurements were reproduced by a theoretical model, event generator, or transport code.

9) CEM03.01 and LAQGSM03.01 are completed, benchmarked, and stored as "frozen" at several X-5 and T-16 computers and are ready for incorporation into transport codes MCNP6, MARS, and MCNPX.

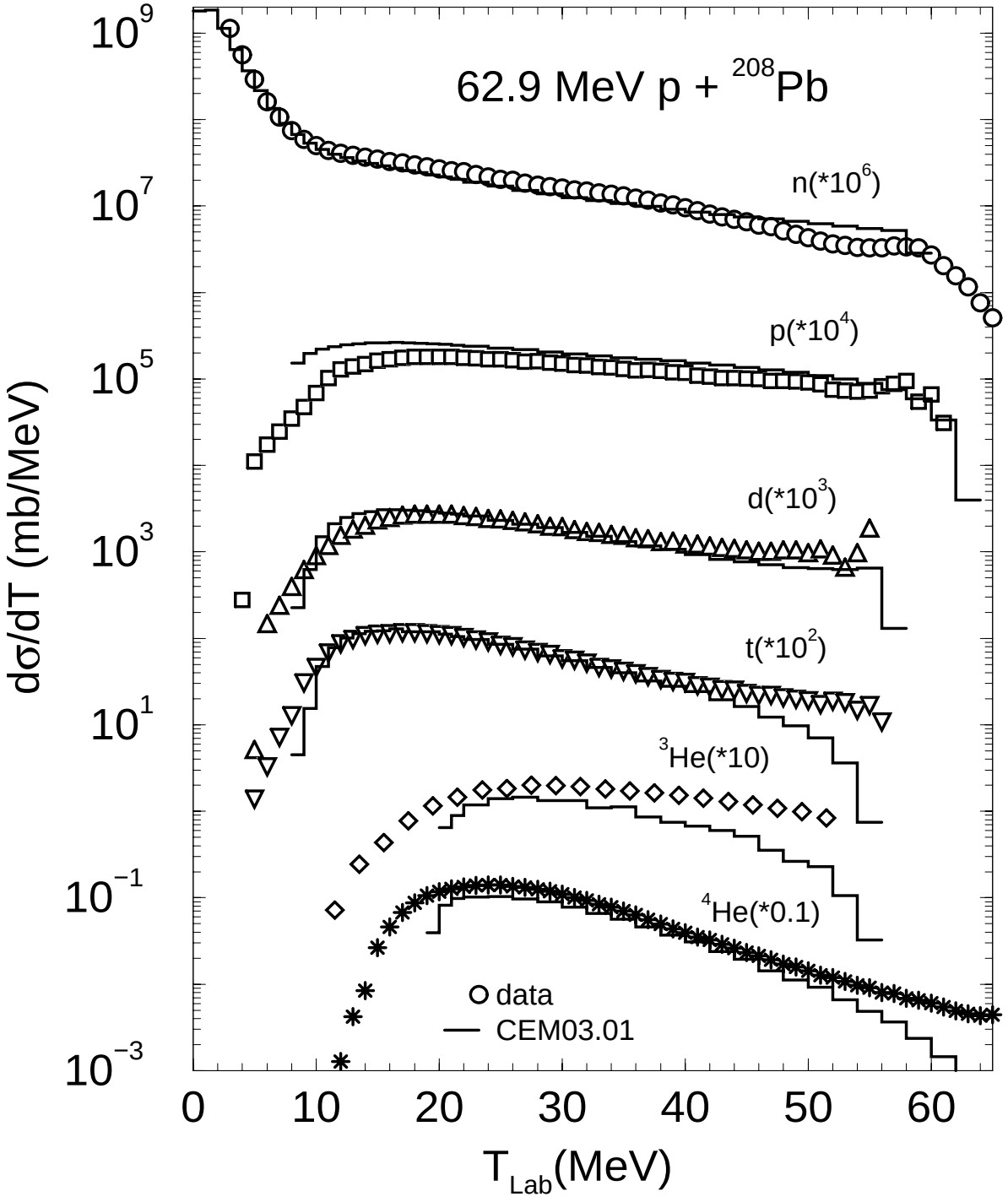


Figure 1: Comparison of CEM03.01 results (histograms) for angle-integrated energy spectra of neutrons and charged particles produced in the reaction 62.9 MeV p + $^{208}$Pb with the recent Louvain-la-Neuve measurements (symbols) [6].

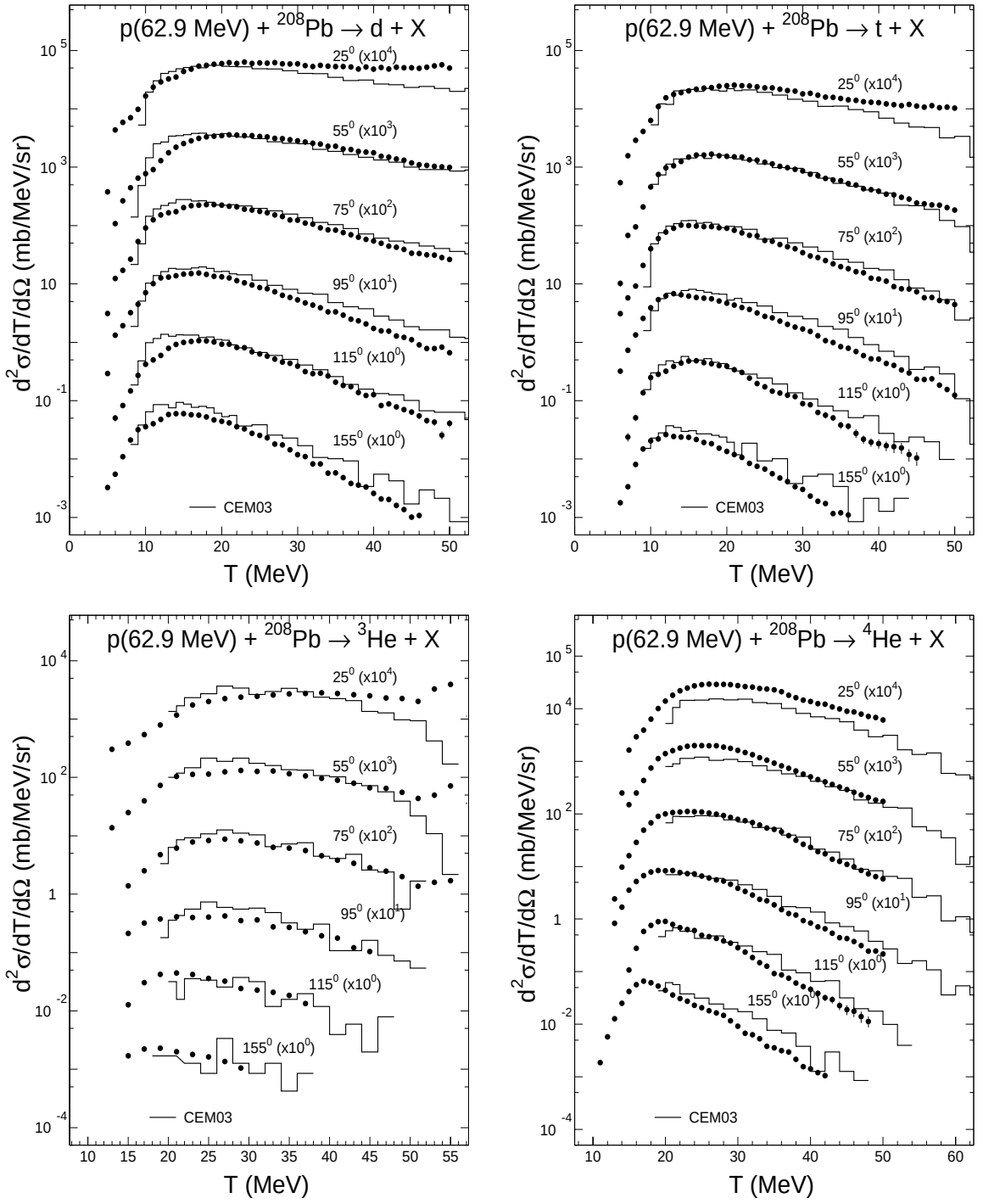


Figure 2: Comparison of CEM03.01 results (histograms) for double-differential spectra of complex particles produced in the reaction 62.9 MeV p + $^{208}$Pb with the recent Louvain-la-Neuve measurements (circles) [6].

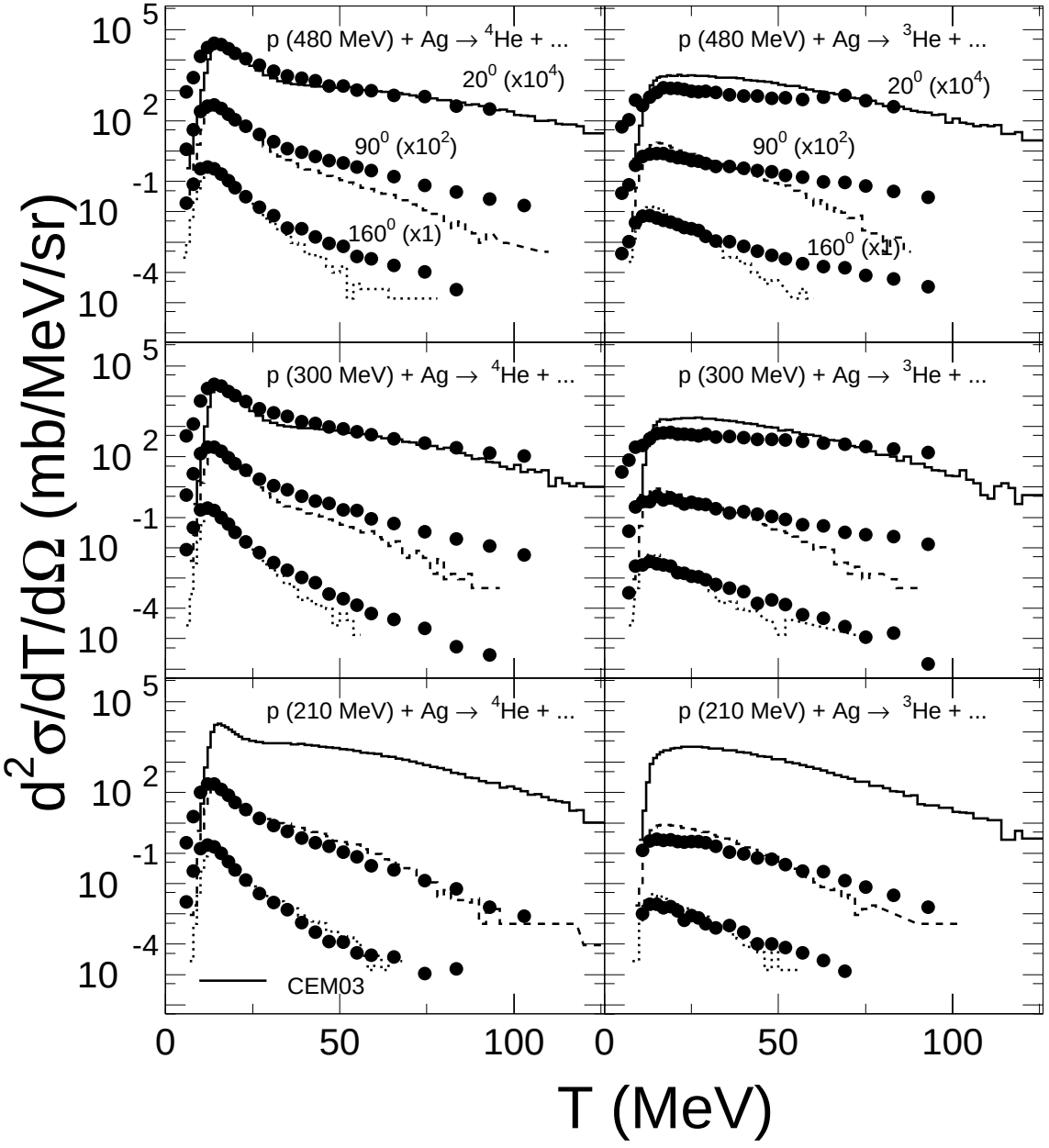


Figure 3: Comparison of CEM03.01 results (histograms) for double-differential spectra of $^3$He and $^4$He produced in interactions of 210, 300, and 480 MeV protons with Ag with experimental data by Green and Korteling (circles) [7].

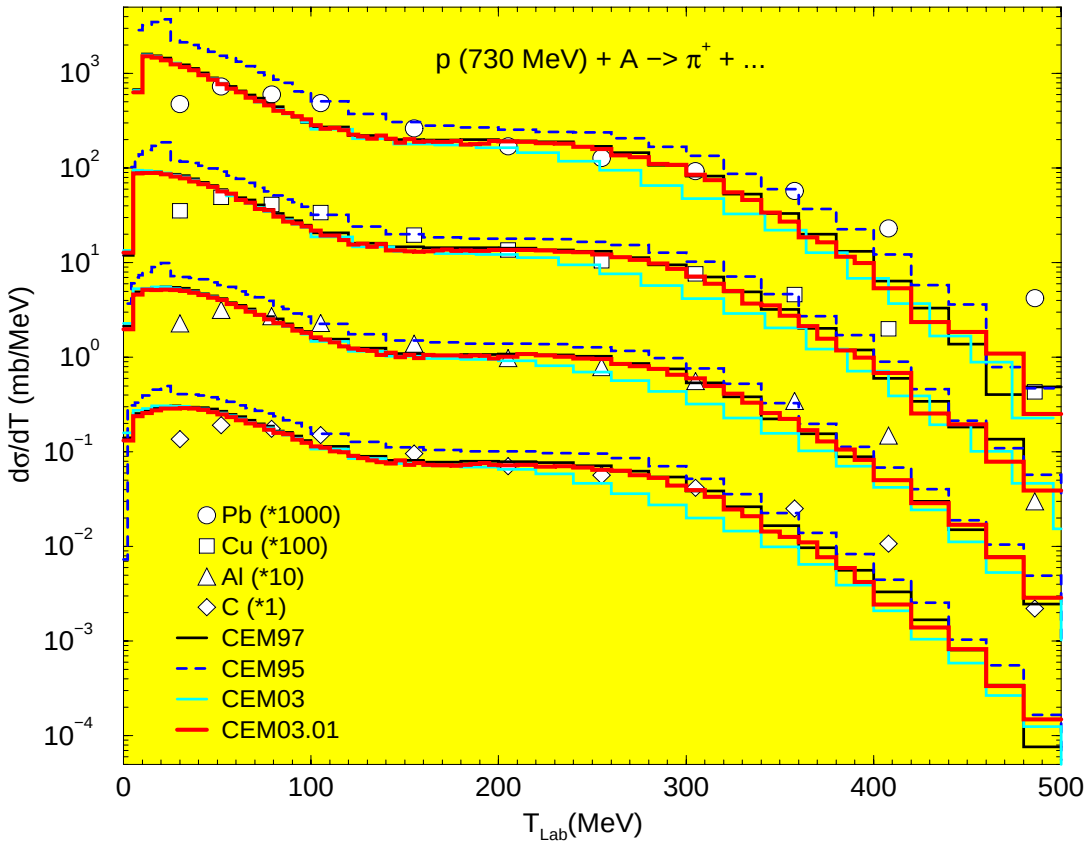


Figure 4: Comparison of CM03.01 results (thick red histograms) for angle-integrated energy spectra of $\pi^+$ produced in interactions of 730 MeV protons with C, Al, Cu, and Pb with experimental data by Cochran *et al.* (symbols) [8] and results from previous versions of the CEM.

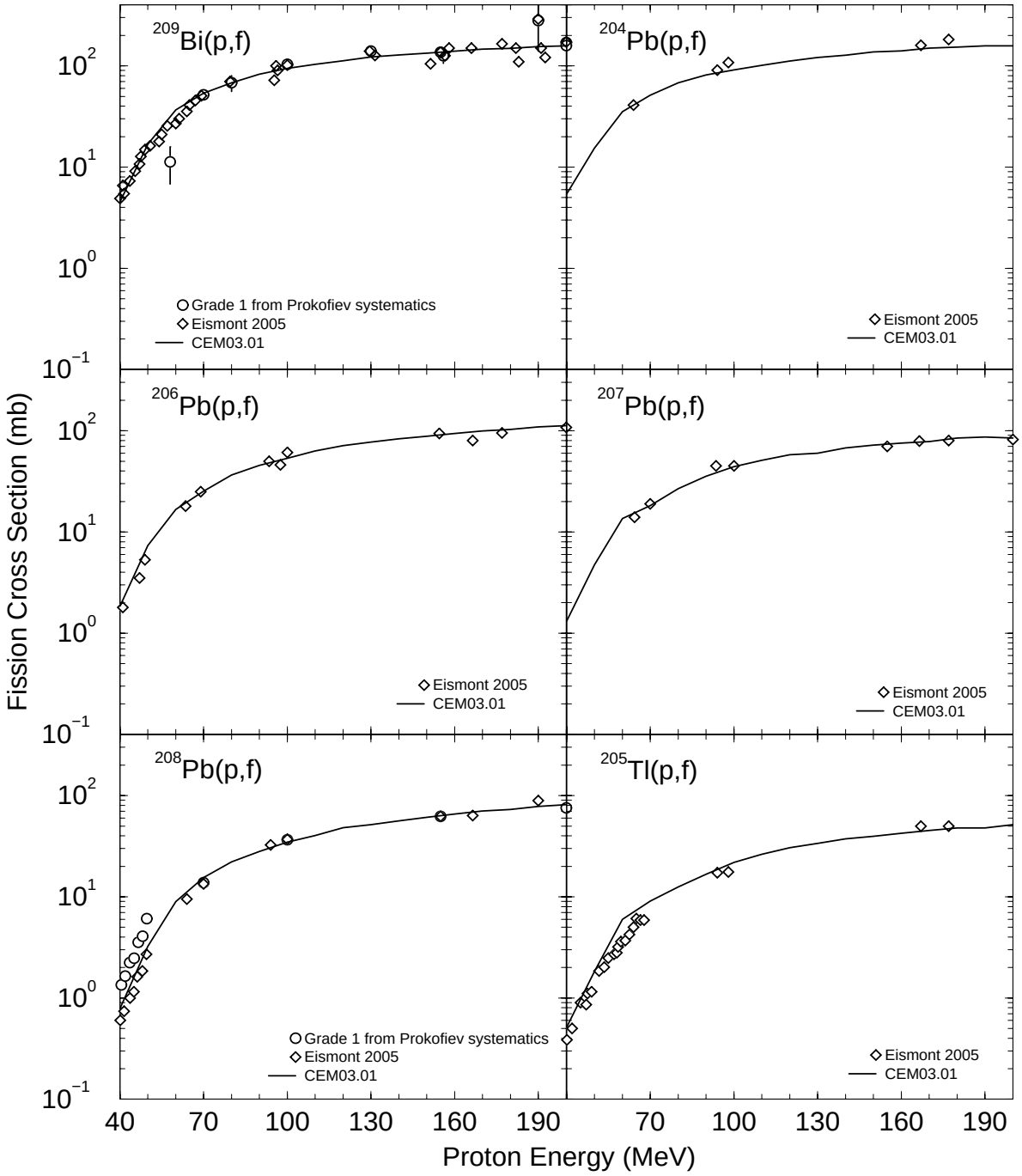


Figure 5: Comparison of CM03.01 results (lines) for proton-induced fission cross sections on $^{209}$Bi, $^{208,207,206,204}$Pb, and $^{205}$Tl with the recent data by Eismont *et al.* (diamonds) [9] and previous measurements from the complication by Prokofiev (circles) [10].

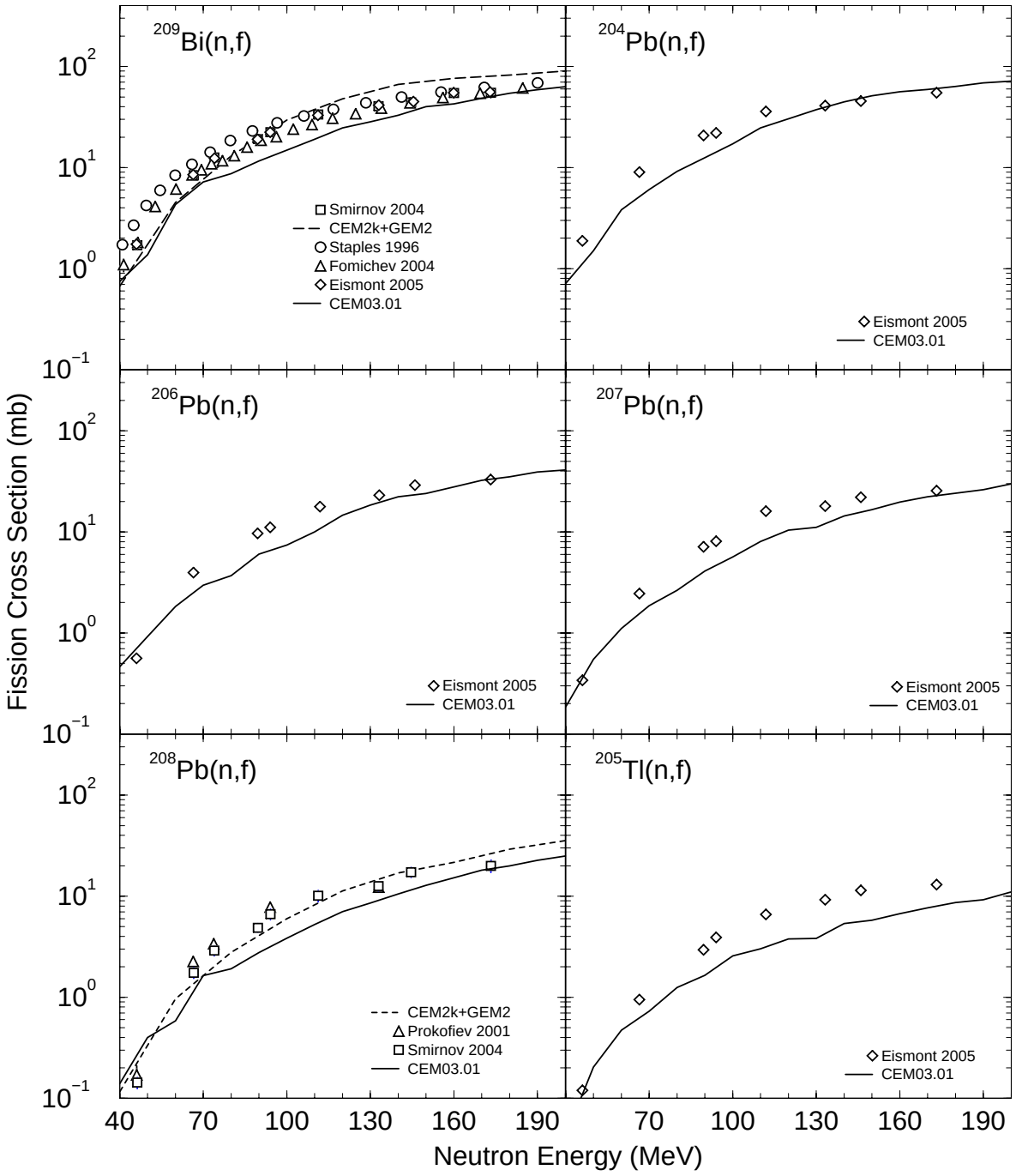


Figure 6: Comparison of CM03.01 results (lines) for neutron-induced fission cross sections on $^{209}$Bi, $^{208,207,206,204}$Pb, and $^{205}$Tl with the recent data by Eismont *et al.* (diamonds) [9], Smirnov *et al.* (squares) [11], Fomichev *et al.* (triangles) [12], Prokofiev *et al.* (triangles) [13], and old LANL measurements by Staples *et al.* (circles) [14].

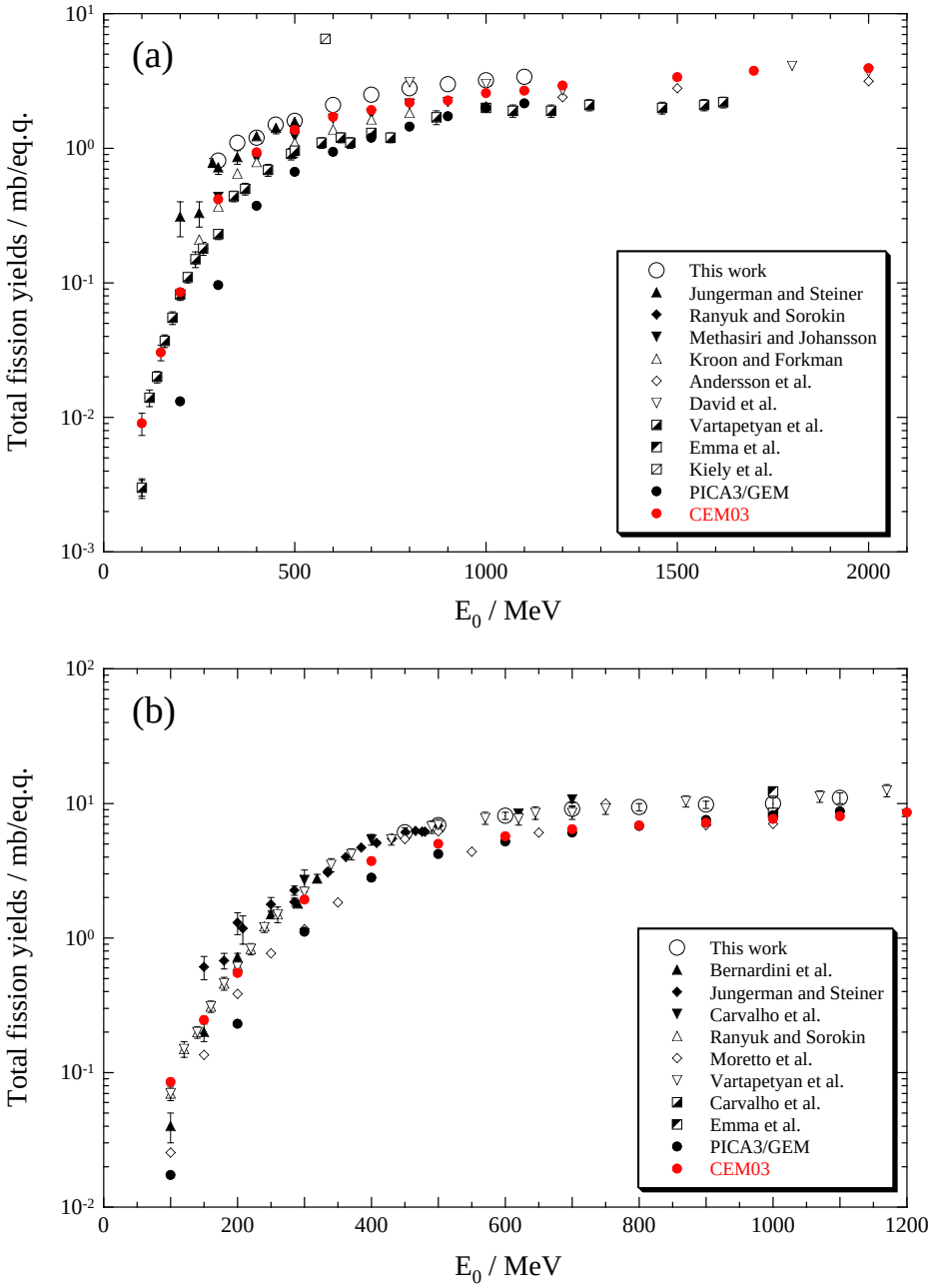


Figure 7: Bremsstrahlung-induced fission cross sections of $^{197}$Au (a) and $^{209}$Bi (b) as functions of the end-point energy $E_0$. All experimental data points, including the ones marked in the legends of the figure as "This work" are from the review by Sakamoto [15]. The CEM03.01 results are shown as solid red circles and marked in the legends as "CEM03". This figure was done for us by Dr. Hiromitsu Haba by adding our CEM03.01 results to Fig. 19 of the review [15].

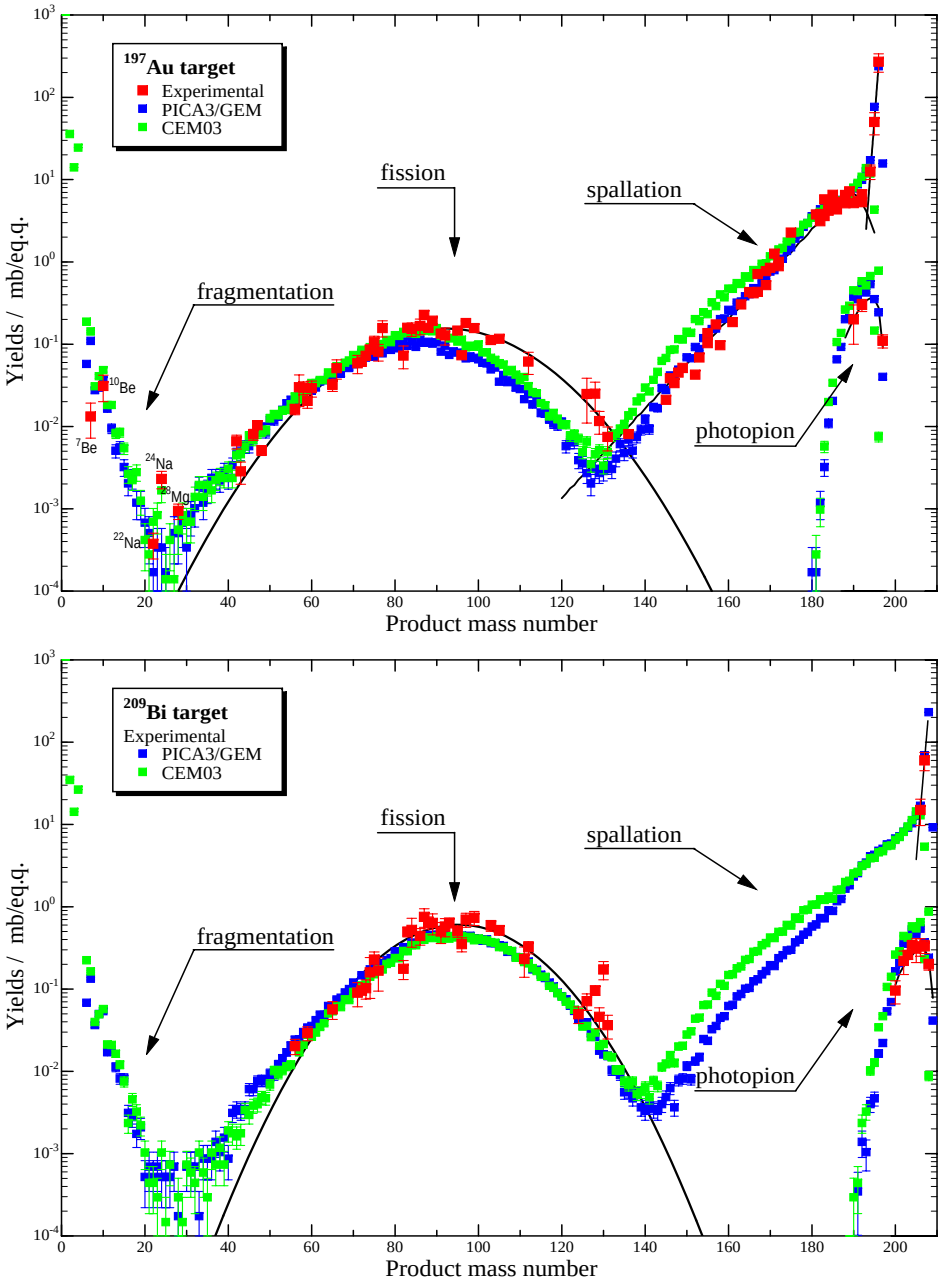


Figure 8: Comparison of CEM03.01 results (green symbols) for the isotopic yields of products produced by bremsstrahlung reactions on $^{197}$Au and $^{209}$Bi at $E_0 = 1$ GeV with experimental data (red symbols) from the review [15] and calculations by PICA3/GEM (blue symbols); the PICA3/GEM results are from several publications and are presented in Fig. 18 of [15] with the corresponding citations. The mass yields for the fission products shown by black curves represent approximations based on experimental data by Prof. Sakamoto's group. This figure was done for us by Dr. Hiroshi Matsumura by adding our CEM03.01 results to Fig. 18 of the review [15].

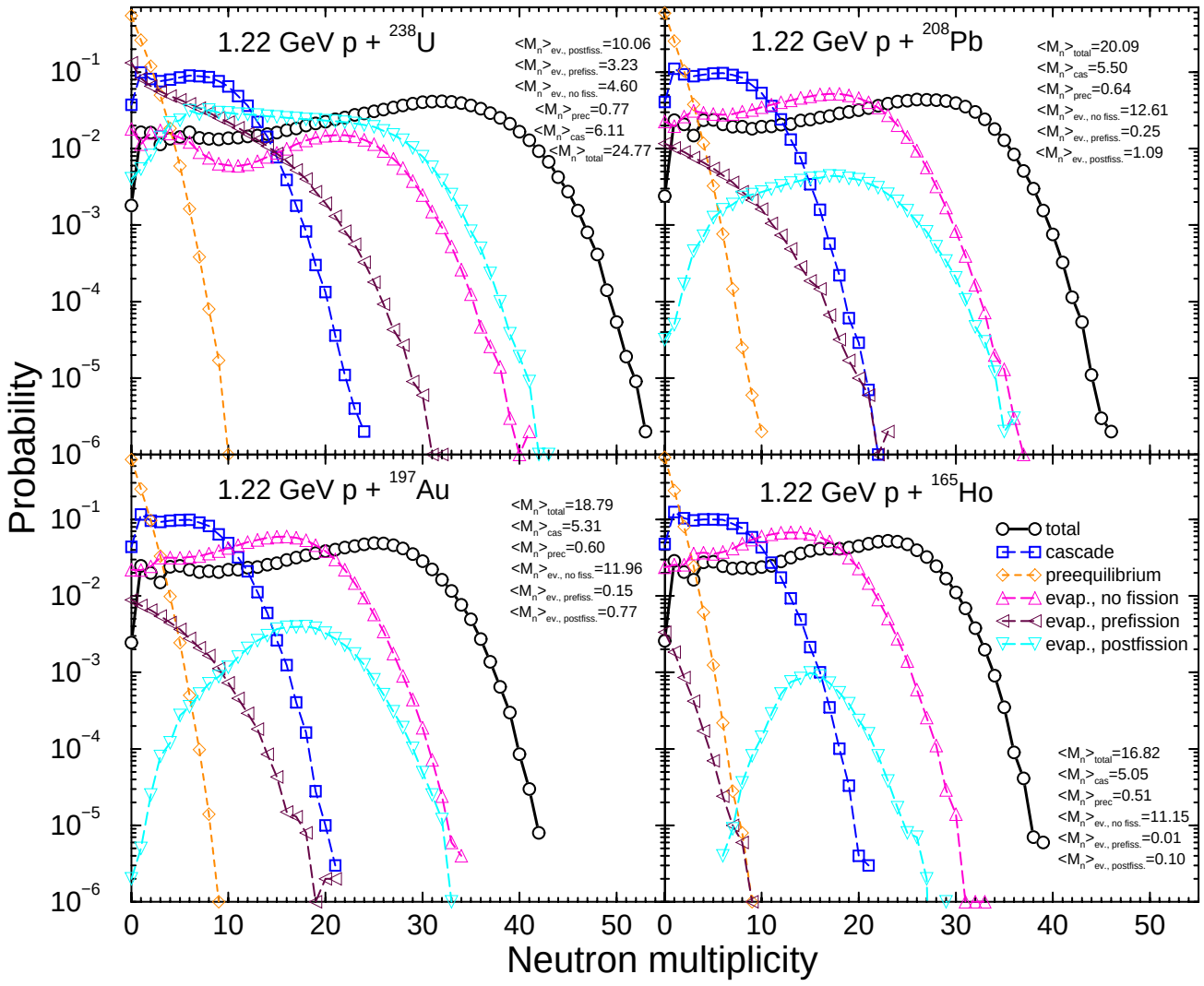


Figure 9: Distributions of neutron multiplicity from interactions of 1.22 GeV protons with $^{238}$U, $^{208}$Pb, $^{197}$Au, and $^{165}$Ho as predicted by CEM03.01. Contributions from the cascade (blue squares), preequilibrium (orange diamonds), evaporation for events without fission (magenta triangles up), evaporation before fission for events with fission (maroon triangles right, "pre-fission"), evaporation from fission fragments (cyan triangles down, "post-fission") mechanisms of reactions as well as their sum (black circles, "total") are shown separately. Mean multiplicities of neutrons for all these reaction mechanisms are noted as $<M_n>$ and shown in the legends of the plots.

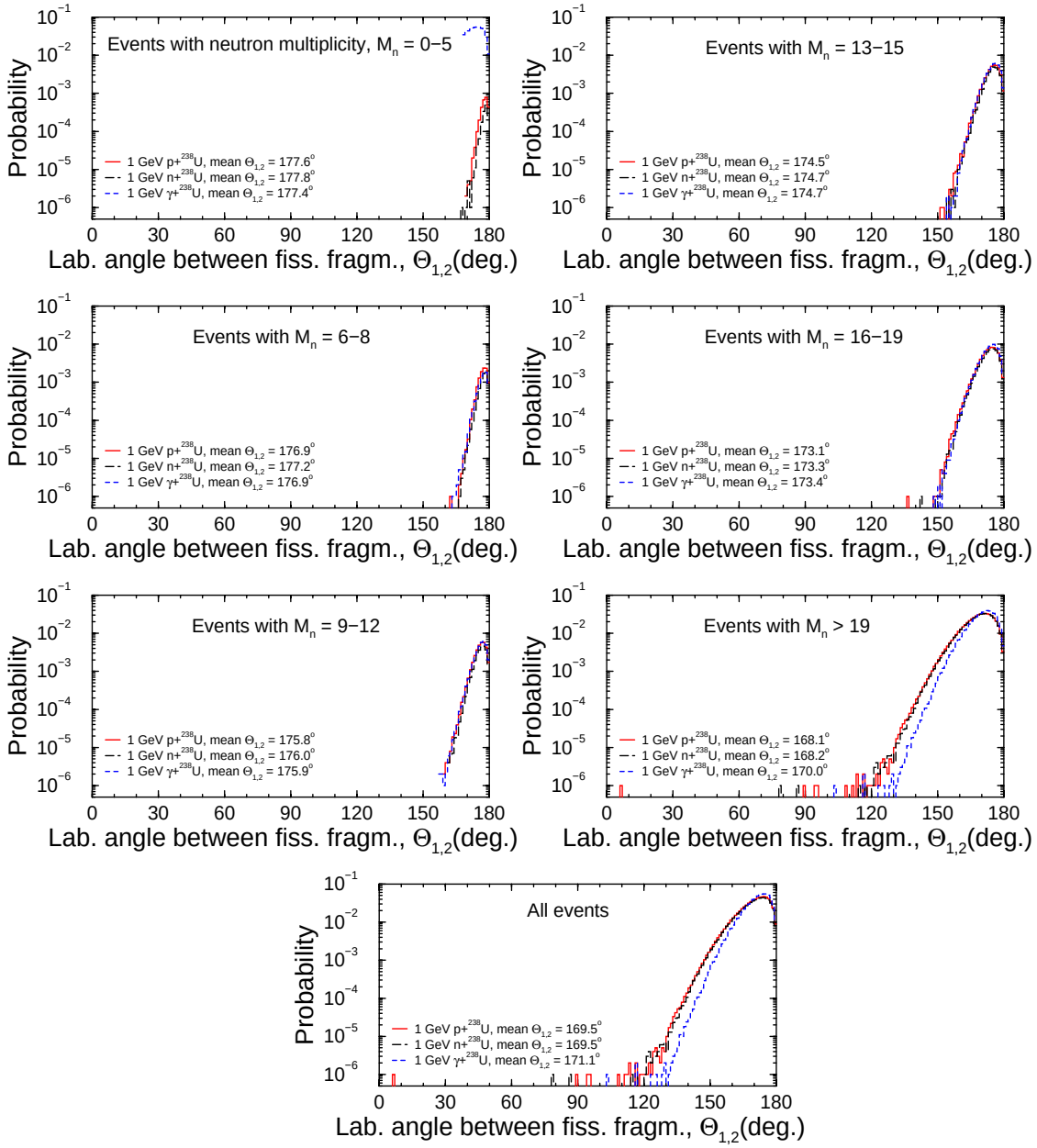


Figure 10: Distributions of angles between the two fission fragments in the laboratory system for 1 GeV proton(solid red histograms)-, neutron(long dashed black histograms)-, and $\gamma$(dashed blue histograms)-induced reactions on $^{238}$U as predicted by CEM03.01. Contributions from events with the mean multiplicities of neutrons $M_n$ from 0 to 5, 6 to 8, 9 to 12, 13 to 15, 16 to 19, and $M_n > 19$, as well as for their sum (all events) are shown on separate plots. The mean laboratory angle between the two fission fragments for all these reactions are shown in the legends of the plots.

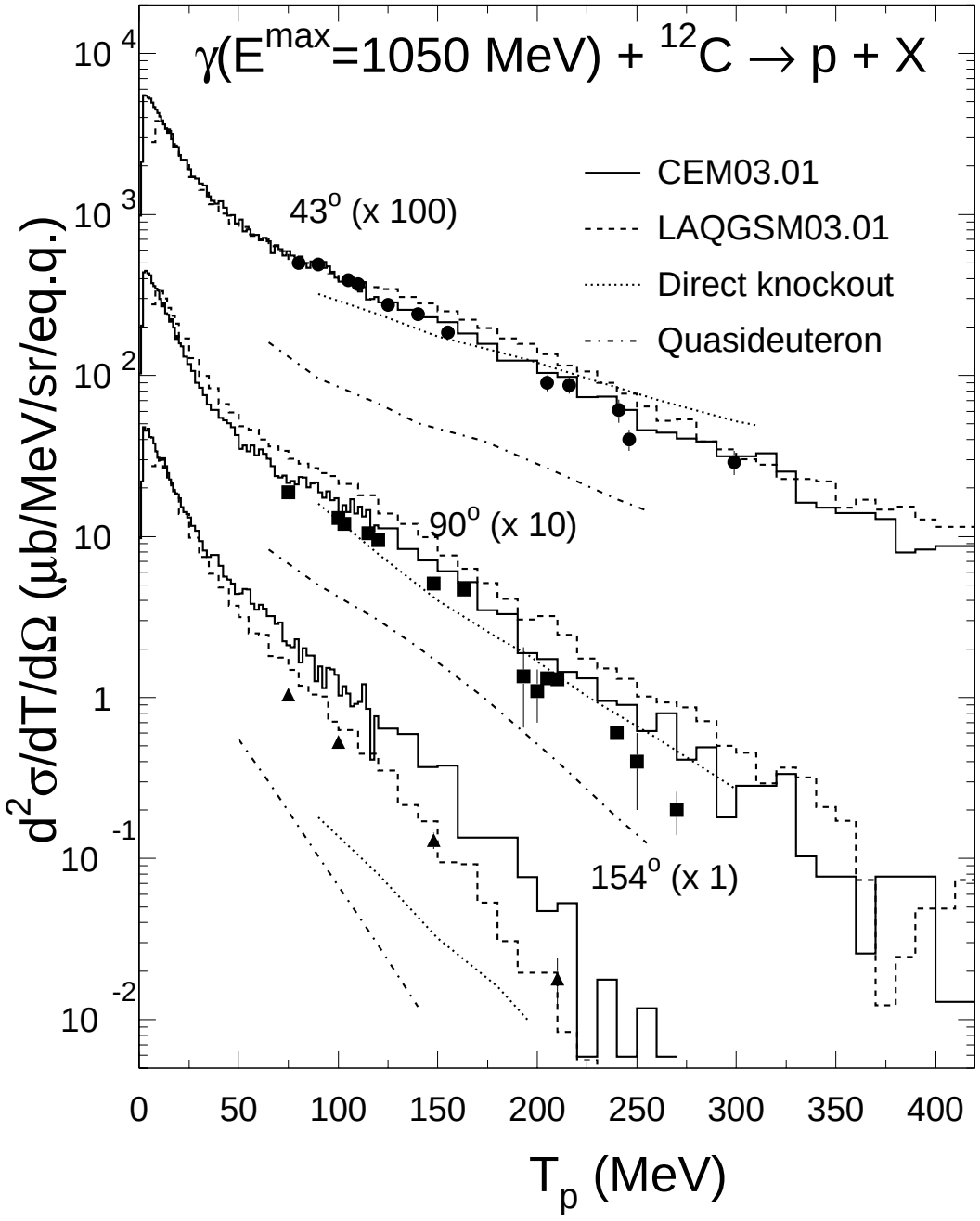


Figure 11: Comparison of measured [17] differential cross section for proton photoproduction on carbon at 43°, 90°, and 154° by bremsstrahlung photons with $E^{max}(\equiv E_0) = 1.05$ GeV (symbols) with CEM03.01 (solid histograms) and LAQGSM03.01 (dashed histograms), and predictions by the direct knockout model [18] (dotted lines) and a quasideuteron calculation [19] (dot-dashed lines), respectively. The experimental data and results by the direct knockout and quasideutron models are taken from Fig. 5 of Ref. [18].

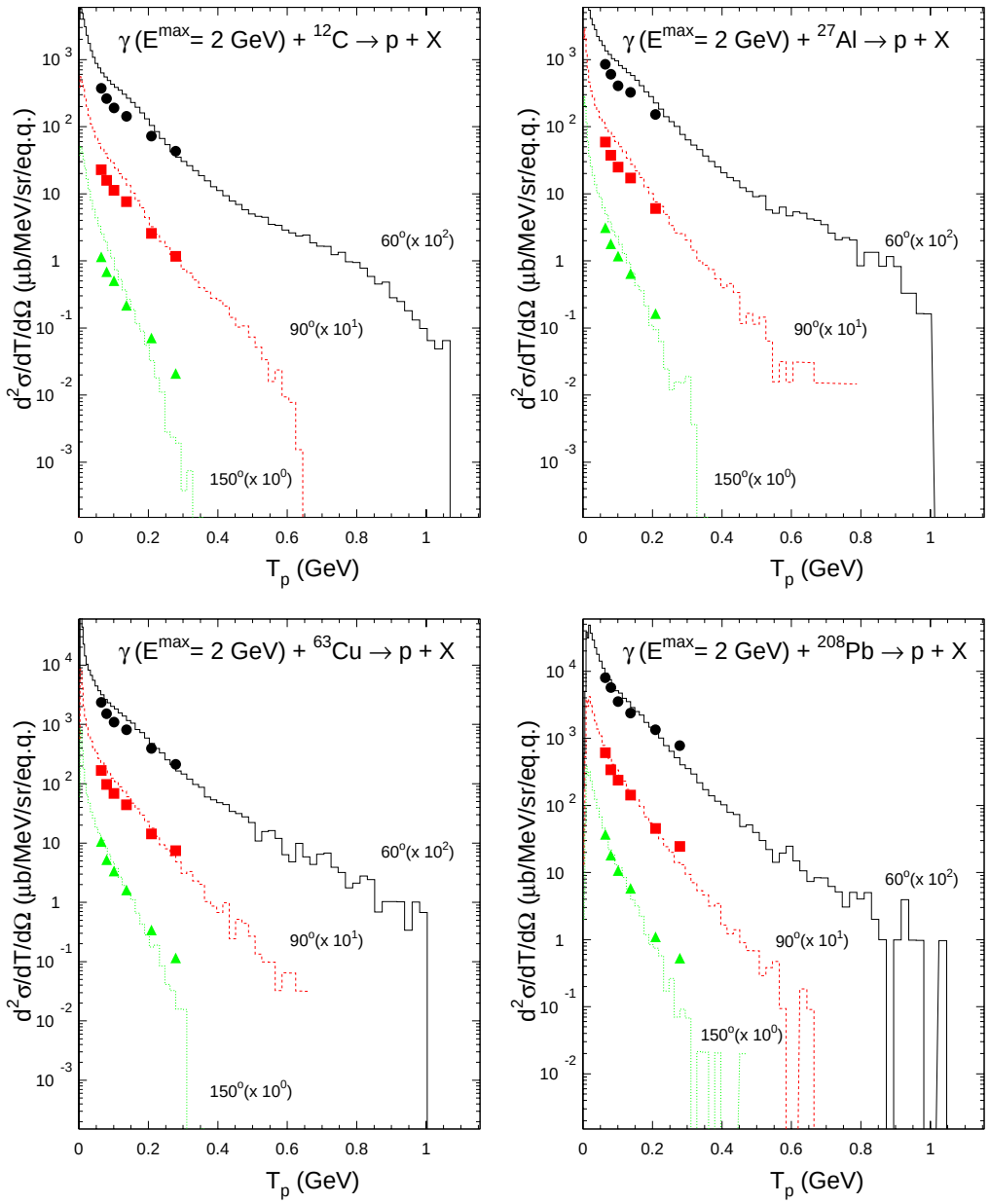


Figure 12: Proton spectra at 60, 90, and 150 degrees from interaction of bremsstrahlung $\gamma$ quanta of maximum energy 2 GeV with $^{12}$C, $^{27}$Al, $^{63}$Cu, and $^{208}$Pb. Experimental values shown by symbols are from [20] while histograms show results by LAQGSM03.01. To the best of our knowledge, we are able to describe these data with LAQGSM03.01 for the first time (see text).

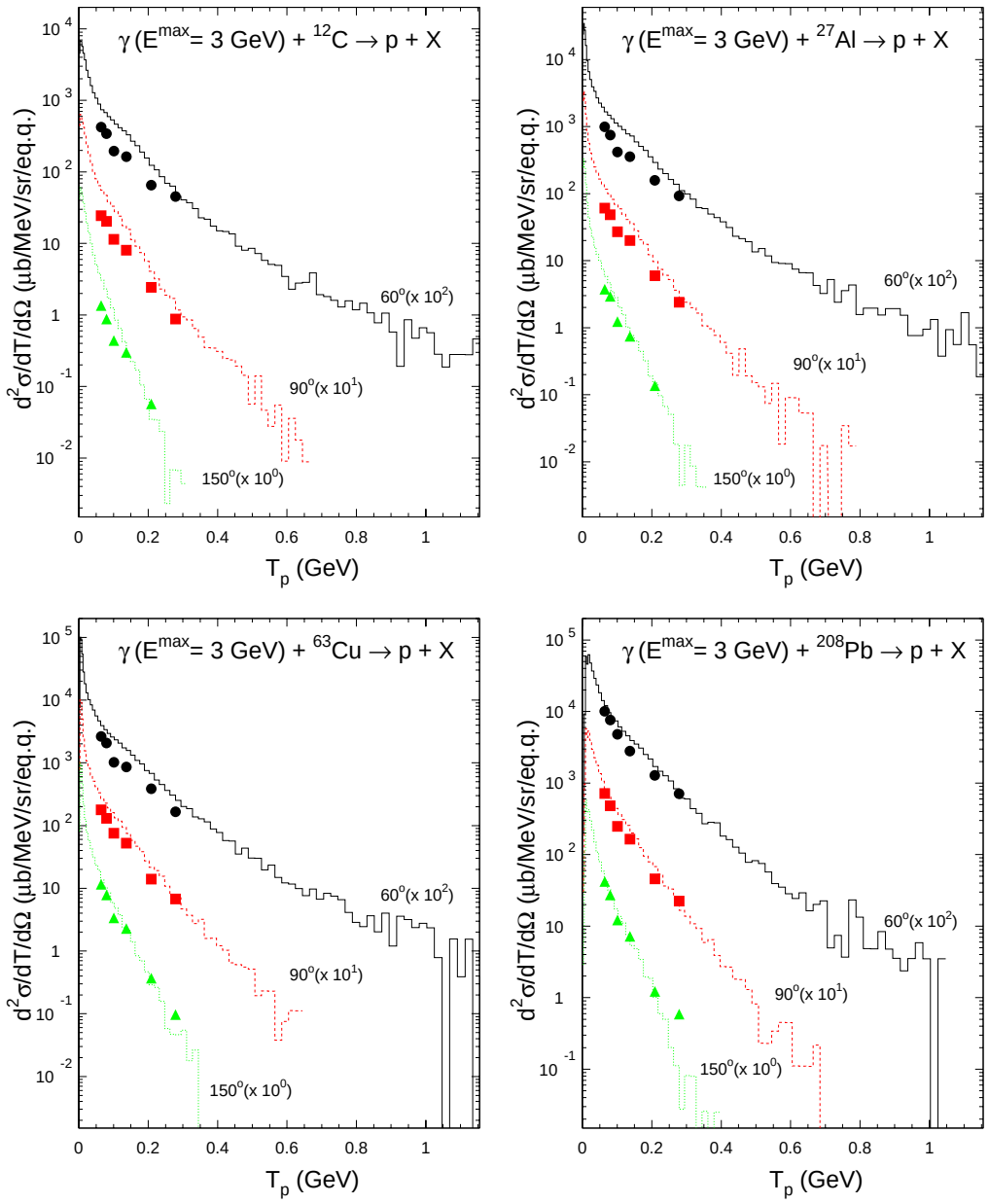


Figure 13: Proton spectra at 60, 90, and 150 degrees from interaction of bremsstrahlung $\gamma$ quanta of maximum energy 3 GeV with $^{12}$C, $^{27}$Al, $^{63}$Cu, and $^{208}$Pb. Experimental values shown by symbols are from [20] while histograms show results by LAQGSM03.01. To the best of our knowledge, using LAQGSM03.01 we are able to describe these data for the first time (see text).

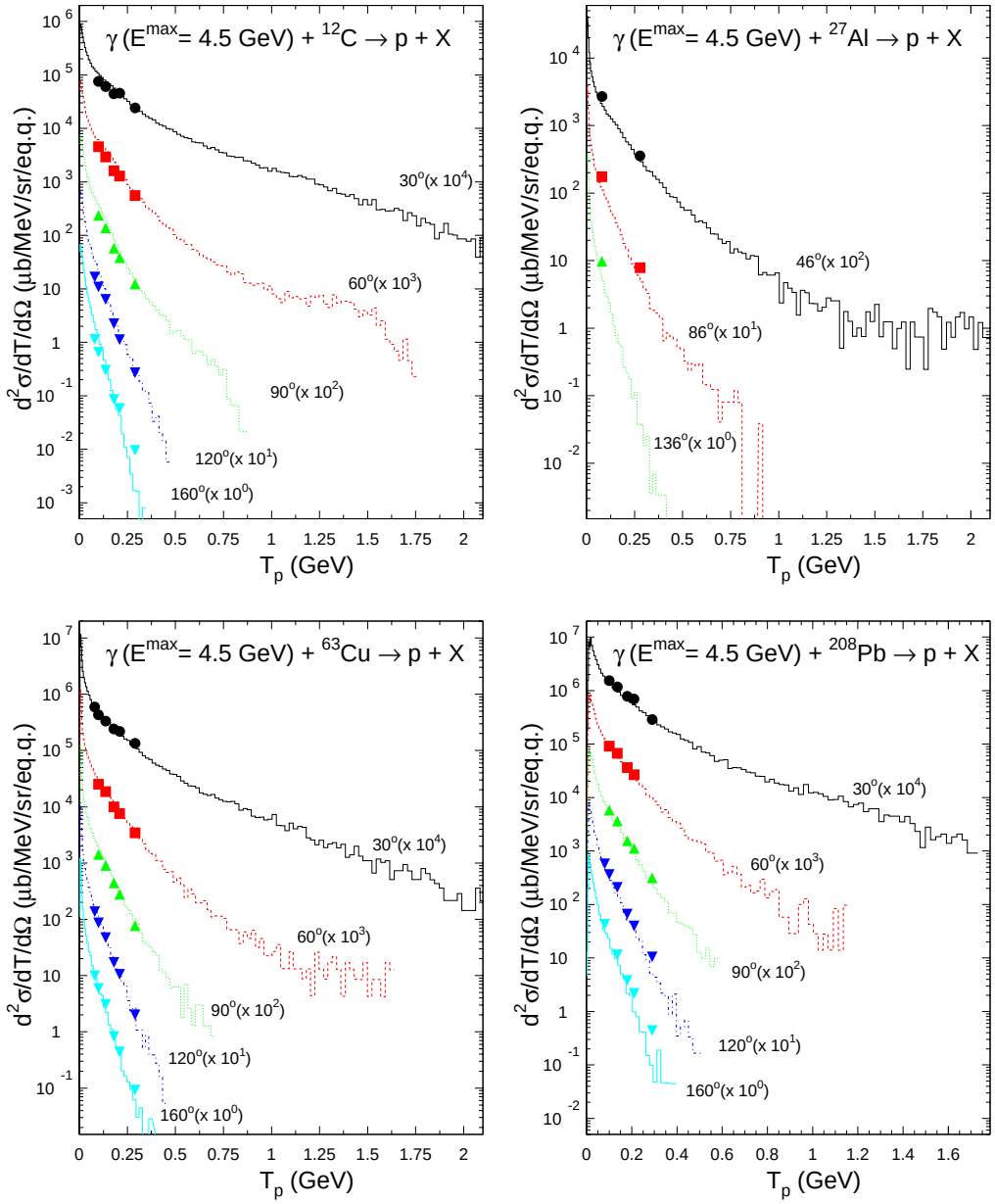


Figure 14: Proton spectra at 60, 90, and 150 degrees from interaction of bremsstrahlung $\gamma$ quanta of maximum energy 4.5 GeV with $^{12}$C, $^{27}$Al, $^{63}$Cu, and $^{208}$Pb. Experimental values shown by symbols are from [20,21] while histograms show results by LAQGSM03.01. To the best of our knowledge, using LAQGSM03.01 we are able to describe these data for the first time (see text).

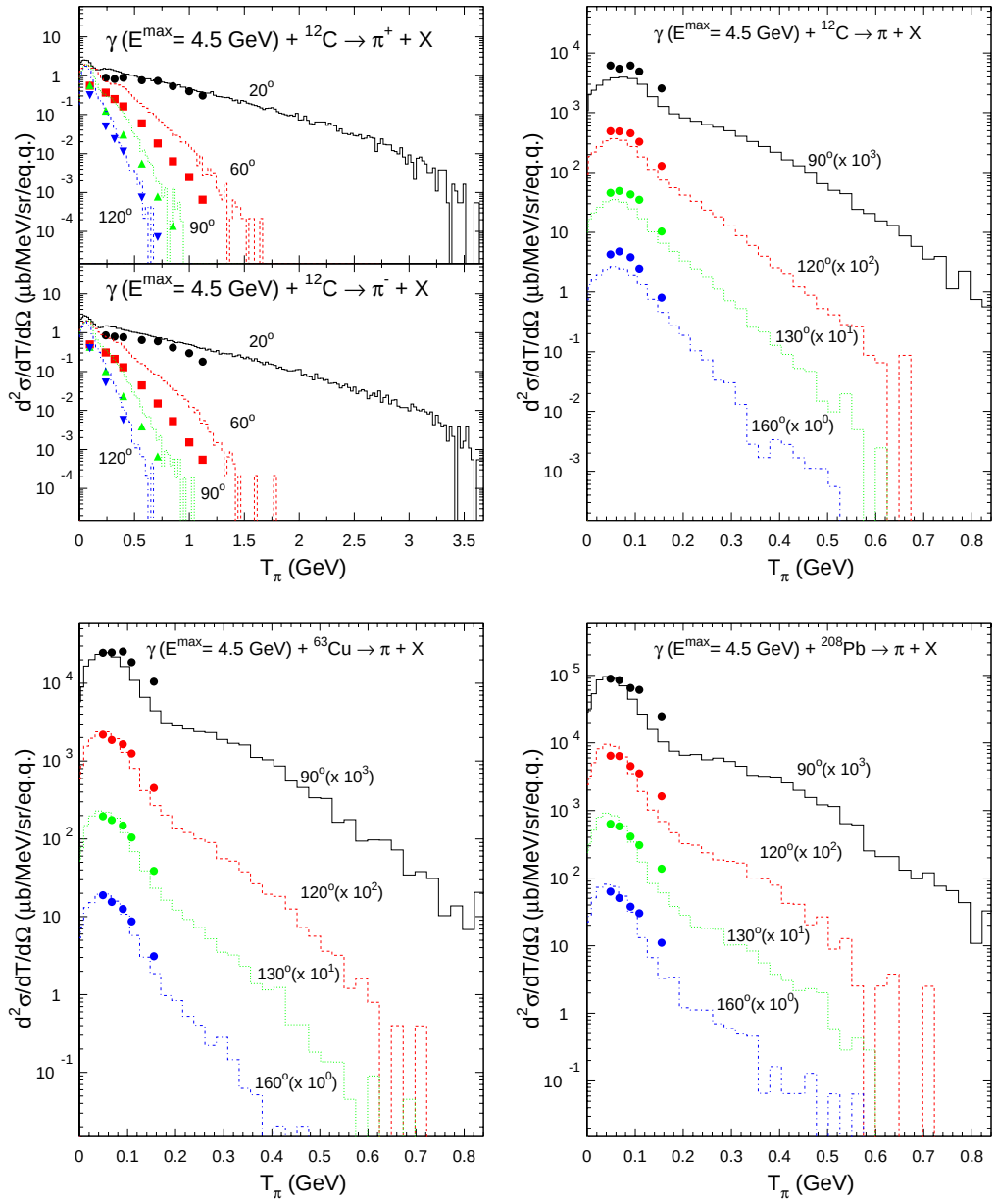


Figure 15: Spectra of positive and negative pions at 20, 60, 90, and 120 degrees produced from the interaction of bremsstrahlung $\gamma$ quanta of maximum energy 4.5 GeV with $^{12}$C (upper left plot) and spectra of charged pions (both $\pi^+$ and $\pi^-$) at 90, 120, 130, and 160 degrees from interaction of the same bremsstrahlung $\gamma$ quanta with $^{12}$C, $^{63}$Cu, and $^{208}$Pb. Experimental data for $\pi^+$ and $\pi^-$ (upper left plot) shown by symbols are from [22] and for pions of both charges from [23], while histograms show results by LAQGSM03.01. To the best of our knowledge, using LAQGSM03.01 we are able to describe these data for the first time (see text).

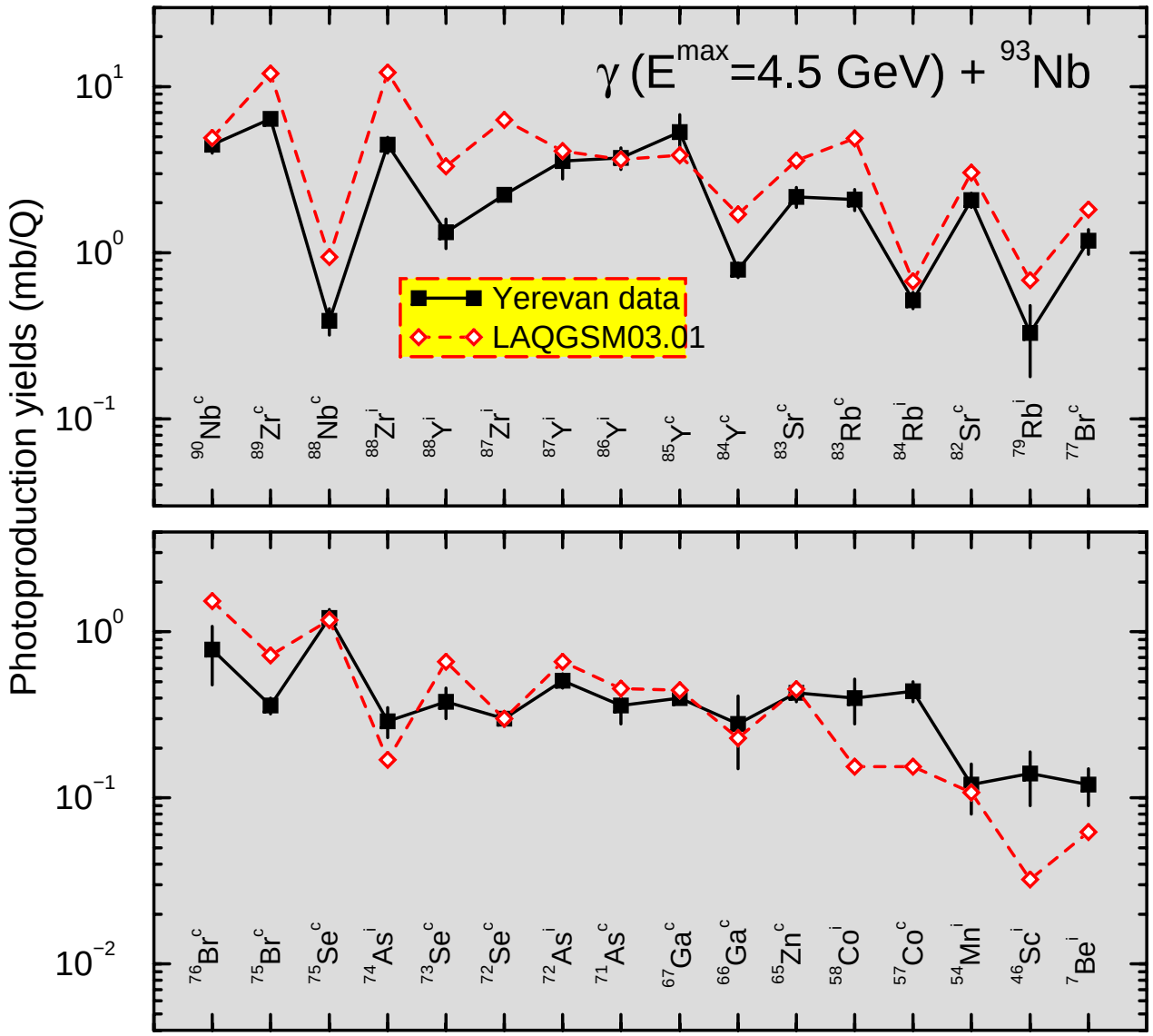


Figure 16: Detailed comparison between experimental yields [24] and those calculated by LAQGSM03.01 of radioactive products from the interaction of bremsstrahlung $\gamma$ quanta of maximum energy 4.5 GeV with $^{93}$Nb. The cumulative yields are labeled as "c" while the independent cross sections, as "i". To the best of our knowledge, using LAQGSM03.01 we are able to describe these data for the first time (see text).

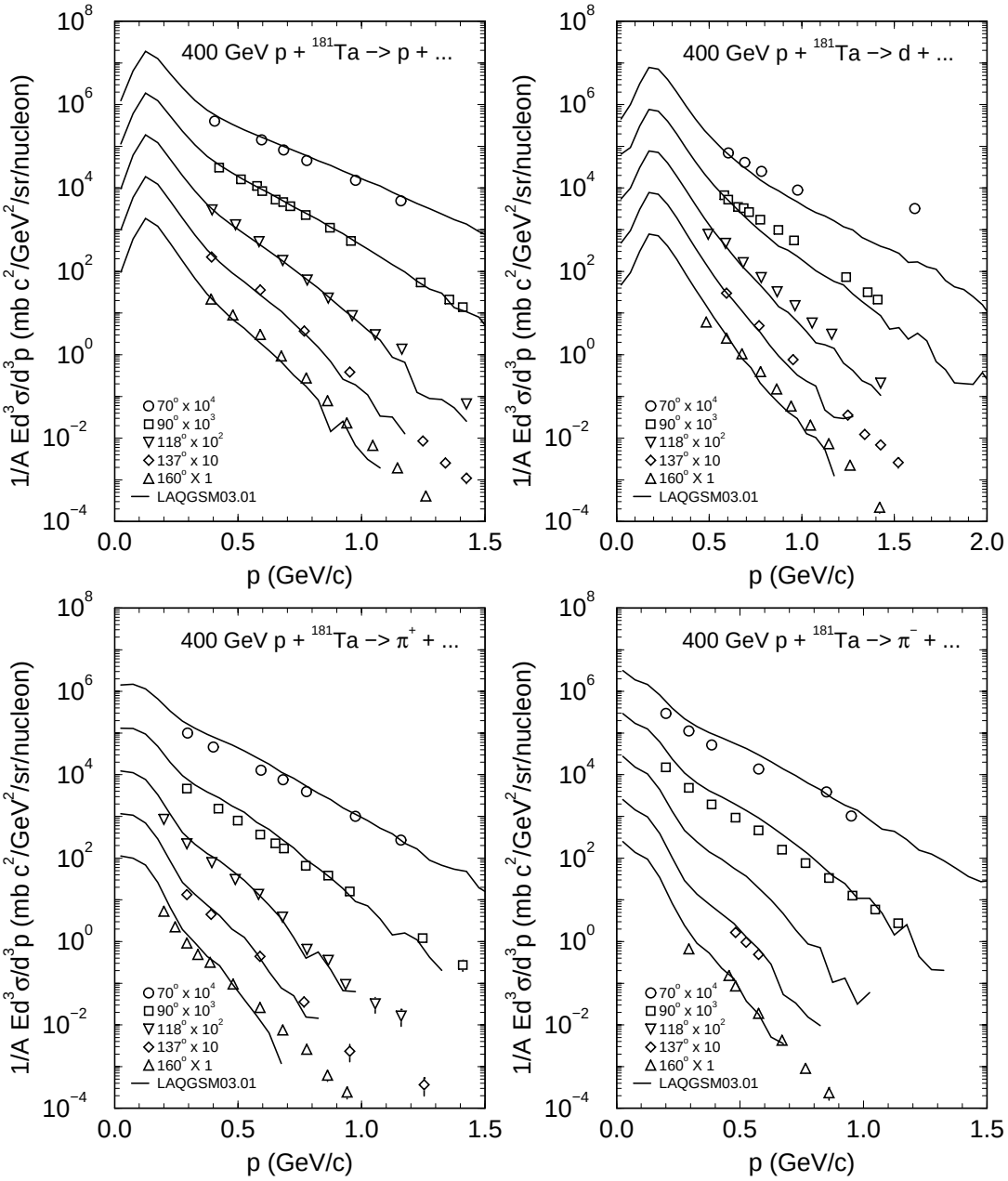


Figure 17: Invariant spectra of p, d, $\pi^+$, and $\pi^-$ from the reaction 400 GeV p + $^{181}$Ta. Experimental data for p are from [25], for d from [26], and for pions from [27]. To the best of our knowledge, using LAQGSM03.01 we are able to describe these data for the first time (see text).

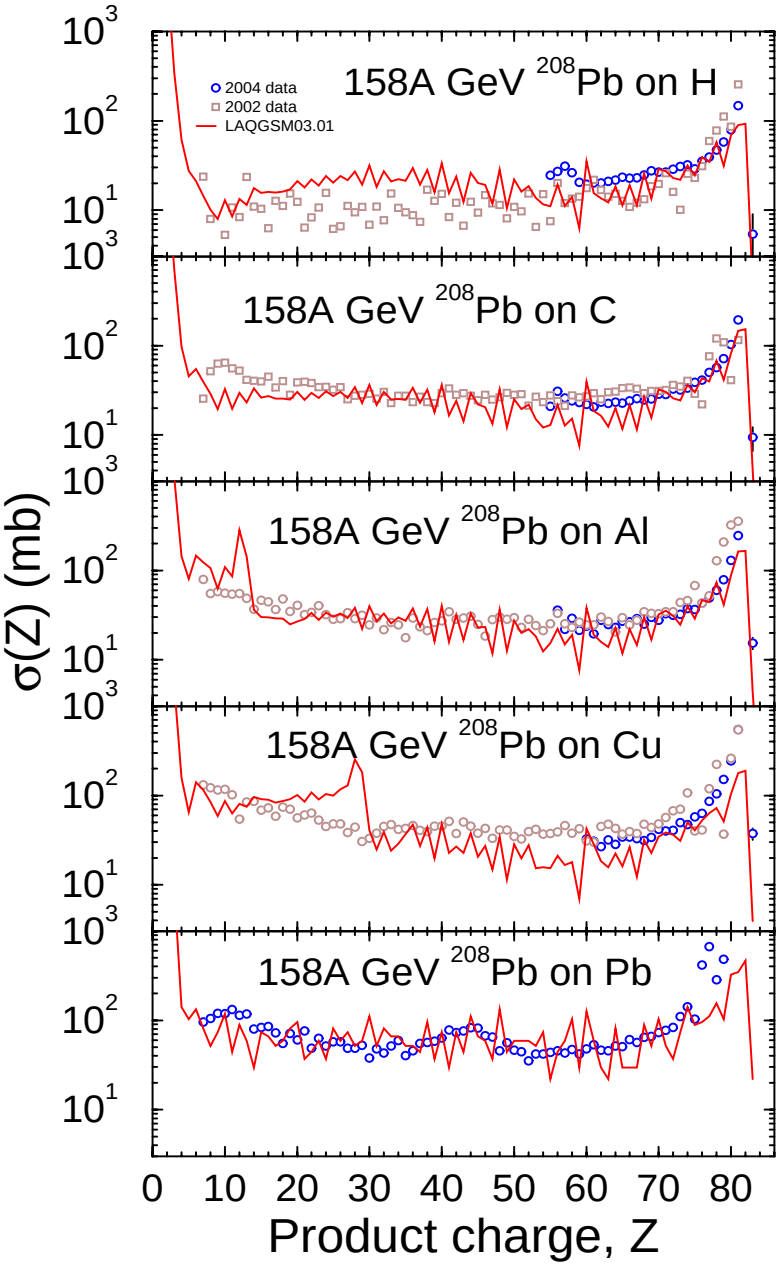


Figure 18: Cross sections for producing an isotope with charge Z by 158A GeV $^{208}$Pb projectiles on p, C, Al, Cu, and Pb targets. Data labeled as 2002 are from [28] (numerical values were kindly sent us by Dr. Alfredo Ferrari), while the 2004 data are from [29]. Our LAQGSM03.01 results (red lines) are only preliminary, with a very low Monte Carlo statistics. Nevertheless, we see clearly a lack of contribution from electromagnetic dissociation to the production of heavy nuclides, as LAQGSM03.01 does not include this process. We would like to address this problem in the next version of LAQGSM.

## Summary

CEM03.01 and LAQGSM03.01 versions of the improved Cascade-Exciton Model (CEM) and Los Alamos Quark-Gluon String Model (LAQGSM) codes have been developed, completed, benchmarked, and stored as "frozen" at several X-5 and T-16 computers and are ready for incorporation into transport codes MCNP6, MARS, and MCNPX and to be delivered to the Radiation Safety Information Computational Center (RSICC) at Oak Ridge in the near future, when we complete writing a User Guide for CEM03.01 and get an LA-UR number for it.

REFERENCES

[1] S. G. Mashnik, K. K. Gudima, R. E. Prael, and A. J. Sierk, "Analysis of the GSI A+p and A+A Spallation, Fission, and Fragmentation Measurements with the LANL CEM2k and LAQGSM Codes," *Proc. TRAMU@GSI*, GSI-Darmstadt, Germany, 2003, ISBN 3-00-012276-1, Eds: A. Kelic and K.-H. Schmidt, http://www-wnt.gsi.de/tramu/; E-print: nucl-th/0404018.

[2] S. G. Mashnik, K. K. Gudima, I. V. Moskalenko, R. E. Prael, and A. J. Sierk, "CEM2k and LAQGSM as Event Generators for Space-Radiation-Shielding and Cosmic-Ray-Propagation Applications," LA-UR-02-6558, Los Alamos (2002), E-print: nucl-th/0210065, *Advances in Space Research* **34** (2004) 1288–1296.

[3] S. G. Mashnik, K. K. Gudima, A. J. Sierk, and R. E. Prael, "Improved Intranuclear Cascade Models for the Codes CEM2k and LAQGSM," *Proc. ND2004*, Santa Fe, USA, 2004, in press; LA-UR-05-0711, Los Alamos (2005), E-print: nucl-th/0502019.

[4] S. G. Mashnik, M. I. Baznat, K. K. Gudima, A. J. Sierk, and R. E. Prael, "Extension of the CEM2k and LAQGSM Codes to Describe Photo-Nuclear Reactions," LANL Report LA-UR-05-2013, Los Alamos (2005), E-print: nucl-th/0503061.

[5] M. Baznat, K. Gudima, and S. Mashnik, "Proton-Induced Fission Cross Section Calculation with the LANL Codes CEM2k+GEM2 and LAQGSM+GEM2," LANL Report LA-UR-03-3750, *Proc. AccApp'03*, ANS, 2004, pp. 976–985; E-print: nucl-th/0307014.

[6] A. Guertin, N. Marie, S. Auduc, V. Blideanu, Th. Delbar, P. Eudes, Y. Foucher, F. Haddad,T. Kirchner, Ch. Le Brun, C. Lebrun, F. R. Lecolley, J. F. Lecolley, X. Ledoux, F. Lefèbvres, T. Lefort, M. Louvel, A. Ninane, Y. Patin, Ph. Pras, G. Rivière, and C. Varignon, "Neutron and Light-Charged-Particle Productions in Proton-Induced Reactions on $^{208}$Pb at 62.9 MeV," *Eur. Phys. J.*, **A23** (2005) 49–60.

[7] Ray E. L. Green and Ralph G. Korteling, "Implications for Statistical Theories of Fragmentation from Measurements of Ag(p,$^3$He) and Ag(p,$^4$He) at Intermediate Proton Energies," *Phys. Rev. C* **18** (1978) 311–316.

[8] D. R. F. Cochran, P. N. Dean, P. A. M. Gram, E. A. Knapp, E. R. Martin, D. E. Nagle, R. B. Perkins, W. J. Shlaer, H. A. Thiessen, and E. D. Theriot, "Production of Charged Pions by 730-MeV Protons from Hydrogen and Selected Nuclei," *Phys. Rev. D* **6** (1972) 3085–3116.

[9] V. P. Eismont, A. N. Smirnov, H. Condé, J. Blumgren, A. V. Prokofiev, N. Olsson, M. C. Duijvestijn, and A. J. Koning, "Compound Nucleus" Effect in Intermediate Energy Nucleon-Induced Fission," submitted to *Phys. Rev. C*, 2005; Andrey N. Smirnov, Vilen P. Eismont, Nikolay P. Filatov, Sergey N. Kirillov, Jan Blomgren, Henri Condé, Nils Olsson, Marieke Duijvestijn, and Arjan Koning, "Correlation of Intermediate Energy Proton- and

Neutron-Induced Fission Cross Sections in the Lead-Bismuth Region," to be published in *Proc. ND2004*, 2005.

[10] A. V. Prokofiev, "Compilation and Systematics of Proton-Induced Fission Cross-Section Data," *NIM* **A463** (2001) 557–575.

[11] A. N. Smirnov, V. P. Eismont, N. P. Filatov, J. Blumgren, H. Condé, A. V. Prokofiev, P.-U. Renberg, and N. Olsson, "Measurements of Neutron-Induced Fission Cross Sections for $^{209}$Bi, $^{nat}$Pb, $^{208}$Pb, $^{197}$Au, $^{nat}$W, and $^{181}$Ta in the Intermediate Energy Region," *Phys. Rev. C* **70** (2004) 054603.

[12] A. V. Fomichev, V. N. Dushin, S. M. Soloviev, A. A. Fomichev, and S. G. Mashnik, "Fission Cross Sections for $^{240}$Pu, $^{243}$Am, $^{209}$Bi, $^{nat}$W Induced by Neutrons up to 500 MeV Measured Relative to $^{235}$U," LANL Report LA-UR-05-1533, Los Alamos, 2005.

[13] A. V. Prokofiev, P.-U. Renberg, and N. Olson, "Measurement of Neutron-Induced Fission Cross Sections for $^{nat}$Pb, $^{208}$Pb, $^{197}$Au, $^{nat}$W, and $^{181}$Ta in the Intermediate Energy Region," Uppsala University Neutron Physics Report UU-NF 01#6 (March 2001).

[14] P. Staples, N. W. Hill, and P. W. Lisowski, "Fission Cross Section Ratios of $^{nat}$Pb and $^{209}$Bi Relative to $^{235}$U for Neutron Energies from Threshold to 400 MeV," *Bull. Am. Phys. Soc.*, **40** (1995) 962; Parrish Staples and Kevin Morley, "Neutron-Induced Fission Cross-Section Rations for $^{239}$Pu, $^{240}$Pu, $^{242}$Pu, and $^{244}$Pu Relative to $^{235}$U from 0.5 to 400 MeV," *Nucl. Sci. Eng.* **129** (1998) 149–163, and private communication from P. Staples to T-2, LANL, 1996.

[15] Koh Sakamoto, "Radiochemical Study on Photonuclear Reactions of Complex Nuclei at Intermediate Energies," *J. Nucl. Radiochem. Sci.* **4** (2003) A9–A31.

[16] A. S. Iljinov, I. A. Pshenichnov, N. Bianchi, E. De Sanctis, V. Muccifora, M. Mirazita, and P. Rossi, "Extension of the Intranuclear Cascade Model for Photonuclear Reactions at Energies up to 10 GeV," *Nucl. Phys.* **A616** (1997) 575–605.

[17] D. N. Olson, Ph.D. thesis, Cornell University, 1960.

[18] D. H. Boal and R. M. Woloshin, "Role of Direct Emission in Strong and Electromagnetically Induced Inclusive Reactions," *Phys. Rev. C* **23**, 1206–1216 (1981)

[19] J. L. Matthews and W. Turchinetz, LNS Internal Report No. 110, 1966.

[20] K. V. Alanakyan, M. Dzh. Amaryan, R. A. Demirchyan, K. Sh. Egiyan, M. S. Ogandzhanyan, and Yu. G. Sharabyan, "Inclusive Photoproduction of Protons by Bremsstrahlung of Maximum Energy 2.0–4.5 GeV," *Yad. Fiz.* **25** (1977) 545–554 [*Sov. J. Nucl. Phys.* **25** (1977) 292–297].

[21] K. V. Alanakyan, M. Dzh. Amaryan, R. A. Demirchyan, K. Sh. Egiyan, Dzh. V. Karumyan, Zh. L. Kocharova, M. S. Ogandzhanyan, and Yu. G. Sharabyan, "Spectra of Cumulative Protons in the Process $\gamma^{12}\mathrm{C} \rightarrow pX$ at a Bremsstrahlung of Maximum Energy 4.5 GeV," *Yad.*

*Fiz.* **34** (1981) 1494–1503 [*Sov. J. Nucl. Phys.*, **34** (1981) 828–833]; K. V. Alanakyan, M. Dzh. Amaryan, R. A. Demirchyan, K. Sh. Egiyan, M. S. Ogandzhanyan, and Yu. G. Sharabyan, "On the Angular Dependence of Photoprotons from Nuclei Irradiated with $\gamma$-Quanta with Maximum Energy 4.5 GeV," *Nucl. Phys.* **A367** (1981) 429–445.

[22] K. Sh. Egiyan, "Cumulative Photoproduction of Particles on Nuclei," Yerevan Physics Institute Preprint EFI-481(24)-81, Yerevan, 1981 (in Russian).

[23] K. V. Alanakyan, M. Dzh. Amaryan, R. A. Demirchyan, K. Sh. Egiyan, M. S. Ogandzhanyan, Yu. G. Sharabyan, and S. G. Stepanyan, "Angular Dependence of the Low-Energy Photopions in the Back Hemisphere," Yerevan Physics Institute Preprint EFI-481(24)-81, Yerevan, 1981; K. V. Alanakyan, M. Dzh. Amaryan, R. A. Demirchyan, K. Sh. Egiyan, Dzh. V. Karumyan, Zh. L. Kocharova, M. S. Ogandzhanyan, and Yu. G. Sharabyan, "Spectra of $\pi^{\pm}$ Mesons in an Inclusive Reaction $\gamma\mathrm{C} \to \pi X$ Induced by Bremsstrahlung $\gamma$ Quanta with of Maximum Energy 4.5 GeV," *Pis'ma Zh. Eksp. Teor. Fiz.* **32** (1980) 666–669 [*JETP Lett.* **32** (1980) 652–656]; K. V. Alanakyan, M. D. Amaryan, R. A. Demirchyan, K. Sh. Egiyan, Zh. L. Kocharova, M. S. Ogandzhanyan, S. G. Stepanyan, and Yu. G. Sharabyan, "The $A$-dependence of the Photoproduction of Inclusive $\pi^{\pm}$ Mesons," *Yad. Fiz.* **34** (1981) 89–94 [*Sov. J. Nucl. Phys.* **34** (1981) 50–53].

[24] G. A. Vartapetyan, E. O. Grigoryan, A. S. Danagulyan, N. A. Demëkhina, and A. G. Khudaverdyan, "Charge Distribution of Residual Nuclei in Photodisintegration of $^{93}$Nb," *Yad. Fiz.* **34** (1981) 289–298 [*Sov. J. Nucl. Phys.* **34** (1981) 163–168].

[25] Y. D. Bayukov, V. I. Efremenko, S. Frankel, W. Frati, M. Gazzaly, G. A. Leksin, N. A. Nikiforov, C. F. Perdrisat, V. I. Tchistilin, and Y. M. Zaitsev, "Backward Production of Protons in Nuclear Reactions with 400 GeV Protons," *Phys. Rev. C* **20** (1979) 764–772.

[26] S. Frankel, W. Frati, M. Gazzaly, Y. D. Bayukov, V. I. Efremenko, G. A. Leksin, N. A. Nikiforov, V. I. Tchistilin, Y. M. Zaitsev, and C. F. Perdrisat, "Backward Production of Light Ions in the Interaction of 400 GeV Protons with Nuclei," *Phys. Rev. C* **20** (1979) 2257–2266.

[27] N. A. Nikiforov, Y. D. Bayukov, V. I. Efremenko, G. A. Leksin, V. I. Tchistilin, Y. M. Zaitsev, S. Frankel, W. Frati, M. Gazzaly, and C. F. Perdrisat, "Backward Production of Pions and Kaons in the Interaction of 400 GeV Protons with Nuclei," *Phys. Rev. C* **22** (1980) 700–710.

[28] S. Cecchini, G. Giacomelli, M. Giorgini, G. Mandrioli, L. Patrizii, V. Popa, P. Serra, G. Sirri, and M. Spurio, "Fragmentation Cross Sections of 158 A GeV Pb Ions in Various Targets Measured with CR39 Nuclear Track Detectors," *Nucl. Phys.* **A707** (2002) 513–524.

[29] C. Scheidenberger, I. A. Pshenichnov, K. Sümmerrer, A. Ventura, J. P. Bondorf, A. S. Botvina, I. N. Mishustin, D. Boutin, S. Datz, H. Geissel, P. Grafström, H. Knudsen, H. F. Krause, B. Lommel, S. P. Møller, G. Münzenberg, R. H. Schuch, E. Uggerhøj, U. Uggerhøj,C. R. Vane, Z. Z. Vilakazi, and H. Weick, "Charge-Changing Interactions of Ultrarelativistic Pb Nuclei," *Phys. Rev. C* **70** (2004) 014902.

SGM:sgm

Distribution:
Eolus Team
A. R. Heath, X-5, F663
J. S. Sarracino, X-5, F663
S. C. Frankle, X-5, F663
R. C. Little, X-5, F663
R. E. Prael, X-5, F663
J. D. Zumbro, X-5, F663
T. J. Bowles, CSO, A121
M. B. Chadwick, ASC, PADNWP, B283
J. A. Carlson, T-16, B28
E. J. Pitcher, T-16, B243
A. J. Sierk, T-16, B243
R. H. Olsher, HSR-4, J573
T. D. McLean, HSR-4, J573
G. W. McKinney, D-5, K575
J. S. Hendricks, D-5, K575
M. R. James, D-5, K575
L. L. Hixson, ISR-CSSE, D466
K. K. Kwiatkowski, P-23, H803
P. W. Lisowski, LANSCE-DO, H845
A. F. Michaudon, LANSCE-3/A, H855
X-DO file
T-DO file
T-16 file
X-5 file